iScience

CellPress
OPEN ACCESS

Article

Distinct actin–tropomyosin cofilament populations drive the functional diversification of cytoskeletal myosin motor complexes

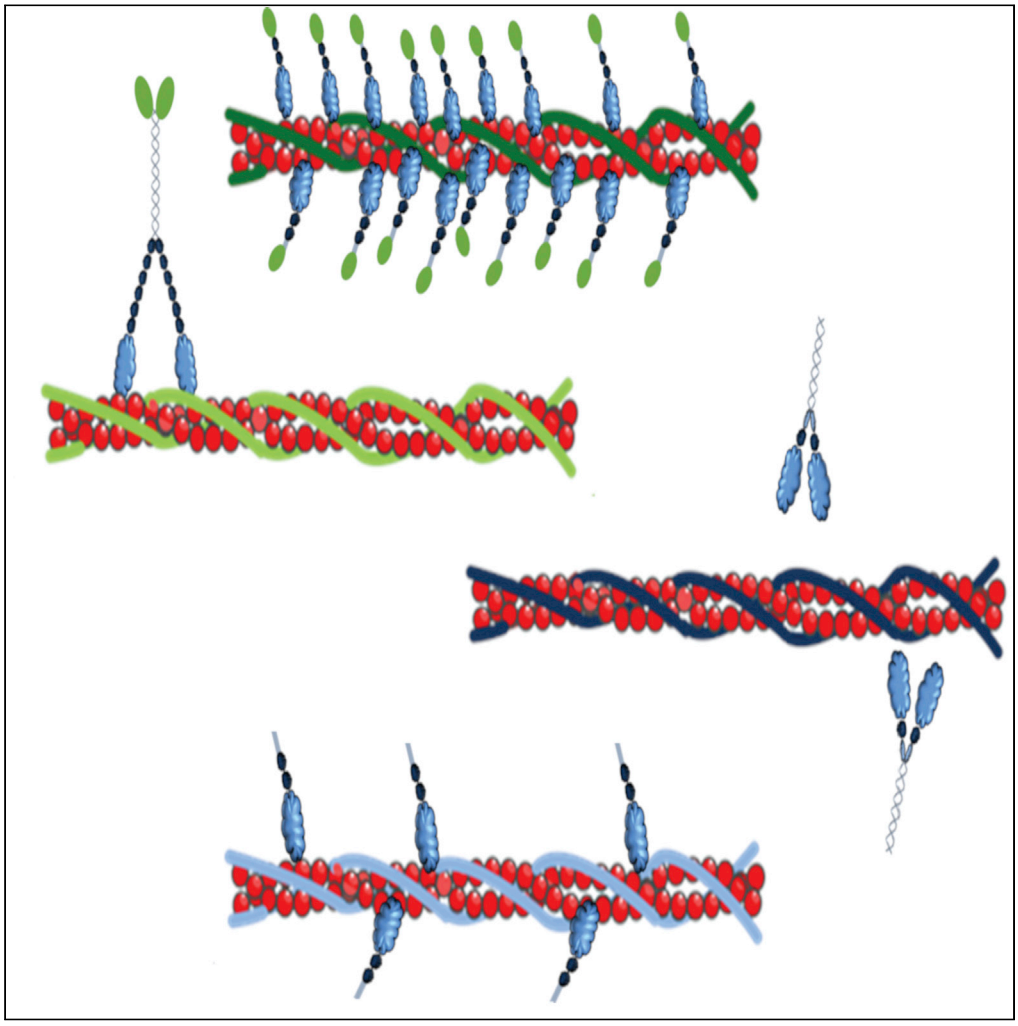

Theresia Reindl, Sven Giese, Johannes N. Greve, ..., Daniel P. Mulvihill, Manuel H. Taft, Dietmar J. Manstein

manstein.dietmar@mh-hannover.de

Highlights

Tpm diversity is largely determined by sequences contributing to the overlap region

Global sequence differences are of greater importance than variable exon 6 usage

Tpm isoforms confer distinctly altered properties to cytoskeletal myosin motors

Cytoskeletal myosins are differentially affected by N-terminal acetylation of Tpm

Reindl et al., iScience *25*, 104484
July 15, 2022
https://doi.org/10.1016/j.isci.2022.104484

iScience

CellPress
OPEN ACCESS

Article

Distinct actin–tropomyosin cofilament populations drive the functional diversification of cytoskeletal myosin motor complexes

Theresia Reindl,[1,5,8] Sven Giese,[1,8] Johannes N. Greve,[1] Patrick Y. Reinke,[1,6] Igor Chizhov,[1] Sharissa L. Latham,[1,7] Daniel P. Mulvihill,[2] Manuel H. Taft,[1] and Dietmar J. Manstein[1,3,4,9,*]

SUMMARY

The effects of N-terminal acetylation of the high molecular weight tropomyosin isoforms Tpm1.6 and Tpm2.1 and the low molecular weight isoforms Tpm1.12, Tpm3.1, and Tpm4.2 on the actin affinity and the thermal stability of actin-tropomyosin cofilaments are described. Furthermore, we show how the exchange of cytoskeletal tropomyosin isoforms and their N-terminal acetylation affects the kinetic and chemomechanical properties of cytoskeletal actin-tropomyosin-myosin complexes. Our results reveal the extent to which the different actin-tropomyosin-myosin complexes differ in their kinetic and functional properties. The maximum sliding velocity of the actin filament as well as the optimal motor density for continuous unidirectional movement, parameters that were previously considered to be unique and invariant properties of each myosin isoform, are shown to be influenced by the exchange of the tropomyosin isoform and the N-terminal acetylation of tropomyosin.

INTRODUCTION

Tropomyosins (Tpm) form a large family of polar, double-stranded, α-helical coiled-coil actin filament binding proteins (McLachlan and Stewart, 1976; von der Ecken et al., 2015). The human Tpm genes are referred to as *TPM1* through *TPM4* (Geeves et al., 2015; Gunning et al., 2008; Lin et al., 1997). Variations in the DNA sequences of the coding regions of the four genes and alternative splicing of the variable exons 1, 2, 6, and 9 give rise to considerable molecular diversity (Figure 1A). As some Tpm splice isoforms are missing variable exon 2, this results in shorter and longer isoforms with 245–248 and 284–285 amino acid residues, respectively. Individual Tpm dimers interact with actin filaments only weakly, with dissociation constants estimated to be in the millimolar range (Tobacman, 2008; Wegner, 1980; Weigt et al., 1991). High-affinity binding occurs only upon polymerization into continuous Tpm cables on the actin filament surface (Fischer et al., 2016; Heald and Hitchcock-DeGregori, 1988; Vilfan, 2001; Wegner, 1980). This process is driven by the head-to-tail association of Tpm dimers (Fischer et al., 2016; Heald and Hitchcock-DeGregori, 1988; Vilfan, 2001; Wegner, 1980), and is further enhanced by the presence of myosin motors (Eaton, 1976; Moraczewska et al., 1999; Pathan-Chhatbar et al., 2018). In general, the dynamic nature of actin–Tpm (A–Tpm) interactions is characterized by high cooperativity and has been shown to influence the competitive association of actin-binding proteins, such as fimbrin and cofilin (Christensen et al., 2017).

Whereas some Tpm isoforms are specifically associated with muscle tissues, most isoforms function within the context of cytoskeletal A–Tpm cofilaments (Gunning et al., 2005; Pittenger et al., 1994). Members of the Tpm family are thought to play a key role in coordinating the interaction of cytoskeletal actin filaments with other types of actin-binding proteins by defining the functional properties of individual actin filament populations. This idea took shape in recent years after it was recognized that almost all actin filaments of the cytoskeleton exist as cofilaments with Tpm isoforms (Meiring et al., 2018) and after various disease associations became known (Marston et al., 2013; Redwood and Robinson, 2013; Reumiller et al., 2018). Specifically, cytoskeletal Tpm isoforms have been linked to diseases affecting neurosensory functions, platelet disorders, and cancer (Brettle et al., 2016; Latham et al., 2018; Pleines et al., 2017). Transformation and cancerous growth are frequently accompanied by upregulated production of low molecular weight (LMW) Tpm isoforms, such as Tpm 3.1 and Tpm4.2, and loss of high molecular weight (HMW) Tpm isoforms (Hendricks and Weintraub, 1981; Kabbage et al., 2013; Stefen et al., 2006, 2018). Thus, over-production of

[1]Institute for Biophysical Chemistry, Fritz–Hartmann–Centre for Medical Research, Hannover Medical School, 30625 Hannover, Germany

[2]School of Biosciences, University of Kent, CT2 7NJ Canterbury, UK

[3]Division for Structural Biochemistry, Hannover Medical School, 30625 Hannover, Germany

[4]RESiST, Cluster of Excellence 2155, Medizinische Hochschule Hannover, 30625 Hannover, Germany

[5]Present address: Department of Microbiology and Immunology, Stanford University School of Medicine, 279 Campus Drive West, Stanford CA 94305, USA

[6]Present address: FS–BMX, Deutsches Elektronen–Synchrotron DESY, Notkestraβe 85, 22607 Hamburg, Germany

[7]Present address: The Kinghorn Cancer Centre, Garvan Institute of Medical Research, 370 Victoria St, Darlinghurst, Sydney, NSW 2010, Australia

[8]These authors contributed equally

[9]Lead contact

*Correspondence: manstein.dietmar@mh-hannover.de

https://doi.org/10.1016/j.isci.2022.104484

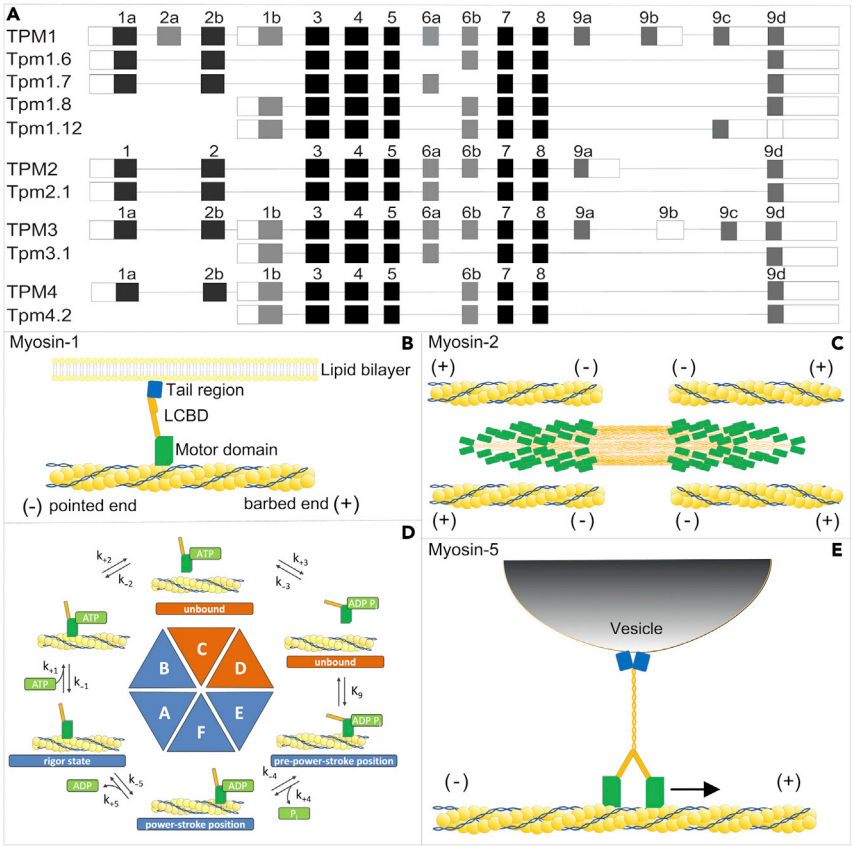

Figure 1. Schematic representations of exon usage for selected Tpm isoforms and the functional context of selected myosin isoforms

(A) Exon usage for Tpm1.6, Tpm1.7, Tpm1.8, Tpm1.12 Tpm2.1, Tpm3.1, and Tpm4.2. Black boxes represent constitutively expressed exons, gray regions represent alternatively spliced coding regions and non-coding regions are shown as white boxes.

(B)–(E) Myosin family motor proteins consist of a generic motor domains (green) followed by a lever arm with light chain binding sites (orange) and the tail region (blue).

(B) Class 1 myosins act in part by connecting membrane lipids with the actin cytoskeleton. They support short range vesicle transport, modulate actin assembly, and function, act as the adaptation motor in the stereocilia of the inner ear, and are implicated in transcription regulation.

(C) The actomyosin ATPase cycle, which is shared by all myosin classes with the exception of class 18, includes the rigor state (state A) and progresses via the following transitions: ATP binding (A→B; K_1), dissociation of the actomyosin complex (B→C; K_2), ATP hydrolysis (C→D; K_3), reassociation with formation of a weak actomyosin complex (D→E, K_9), phosphate release, formation of a strong actomyosin complex and powerstroke (E→F; K_4), ADP release (F→A; K_5), which returns the Myo1C to the rigor state.

(D) Non-muscle myosin-2 isoforms are predominantly organized into stress fibers that are able to generate contractile forces that support functions such as cell adhesion, migration and mechanotransduction.

(E) Class 5 myosin dimers act in part by transporting cargo such as vesicles from the center of the cell toward the periphery. The polarity of the actin filament is indicated as + (barbed) and – (pointed) ends.

Tpm4.2 has been directly linked to the invasiveness of infiltrating breast cancer cells. In transformed cells, Tpm3.1 accounts for up to 70% of total Tpm, as opposed to 25% in corresponding control cells (Meiring et al., 2018). Compounds that manipulate actin function by directly targeting Tpm3.1 are therefore attractive and promising anti-cancer agents (Bonello et al., 2016; Stehn et al., 2013).

The regulation of myosin motor activity by A–Tpm cofilaments differs between sarcomeric and cytoskeletal isoforms. In the context of muscle, calcium binding to troponin triggers a series of conformational changes that shift the Tpm filament on F-actin to reveal the myosin-binding interface on the actin filament (Parry and Squire, 1973; Spudich et al., 1972; Spudich and Watt, 1971). In contrast to the muscle system, cytoskeletal actomyosin

complexes function in the absence of troponin or isofunctional troponin-like proteins and the context of greater Tpm isoform diversity. Cell-based and biochemical studies support the hypothesis that the association of filamentous actin with different tropomyosin isoforms determines the identity and modulates the activity of the interacting myosin motor proteins (Gateva et al., 2017; Manstein and Mulvihill, 2016). Specifically, it has been shown that bipolar bundles of non-muscle myosin-2 (NM-2) isoforms that function as integral components of stress fibers, actin arcs, and contractile rings, and the various unconventional myosin motors that support vesicle and organelle transport, as well as discrete steps of endocytosis and exocytosis, are integrated into the appropriate functional context by distinct A–Tpm cofilaments as schematically shown in Figures 1B–1E (Barua et al., 2018; Clayton et al., 2015; Kee et al., 2015; Meiring et al., 2019; Sckolnick et al., 2016).

Corroborating evidence includes the observation that class 1 myosin-dependent delivery of organelles to the perinuclear region is affected by the association of F-actin with Tpm1.7 but not with Tpm3.1 (Pelham et al., 1996). Cargo structures that carry myosin-1C (Myo1C) on their surface are regulated by Tpm1.6 with respect to their run initiation and run termination, which may enable effective sorting of cargo by co-regulation of the initiation and termination of kinesin-driven runs at actin/microtubule intersections (McIntosh et al., 2015). In the cortical region of adipocytes, Tpm3.1 but not Tpm1.7 was proposed to define the actin population regulating the recruitment of Myo1C and non-muscle myosin-2A (NM-2A), which are both required for GLUT4-mediated glucose uptake and blood glucose clearance (Kee et al., 2015). In stress fibers, the incorporation of the HMW splice isoforms Tpm1.6 and Tpm2.1 produces opposite effects with respect to NM-2-dependent force development, with Tpm1.6 causing an increase in intracellular pressure, whereas incorporation of Tpm2.1 decreases traction force (Sao et al., 2019). In addition, Tpm2.1 has a specific role that other Tpm isoforms cannot replace, supporting correct rigidity sensing and detection of tensile stress at the cell periphery (Wolfenson et al., 2016). The incorporation of both LMW isoforms Tpm3.1 and 4.2 into stress fibers promotes the specific recruitment of NM-2A (Bryce et al., 2003). Cofilaments formed by F-actin and Tpm3.1 or Tpm4.2 are characterized by rapid dynamic exchange and are not effectively protected from disassembly (Gateva et al., 2017). NM-2A NM-2A was shown to have increased sliding velocity and ATPase activity in complex with actin–Tpm3.1 (Barua et al., 2014) and actin–Tpm4.2 cofilaments (Hundt et al., 2016). Moreover, the association of actin filaments with Tpm3.1 or Tpm4.2 has been shown to increase ATP turnover by NM-2A and NM-2B ATPase owing to a specific acceleration of the rate-limiting step of phosphate release. Under resisting force conditions, actin–Tpm3.1 and actin–Tpm4.2 cofilaments induce a slower release of the hydrolysis product ADP, leading to an increase in duty-cycle and processive behavior of NM-2B and NM-2A (Hundt et al., 2016; Pathan-Chhatbar et al., 2018).

In the case of cytoskeletal Tpm isoforms without N-terminal acetylation, apparent affinities for filamentous actin in the range of 0.1–5 μM have been reported for Tpm1.6, Tpm1.7, Tpm1.8, Tpm2.1, Tpm3. 1, and Tpm4.2. No clear correlation was found between affinity and size of Tpm isoforms (Carman et al., 2021; Janco et al., 2016; Moraczewska et al., 1999; Ngo et al., 2016). It is known that N-terminal acetylation is important for the ability of sarcomeric Tpm isoforms to interact with F-actin, but less critical for the binding of the cytoskeletal Tpm isoforms (Meiring et al., 2018; Palm et al., 2003). Biochemical and structural biology studies suggest that N-terminal acetylation of Tpm isoforms not only acts locally but has consequences for conformational dynamics far from the Tpm N-terminus and thus on the function and stability of A–Tpm cofilaments (East et al., 2011; Greenfield et al., 1994; Johnson et al., 2018; Monteiro et al., 1994; Palm et al., 2003). In the case of muscle-specific isoforms Tpm1.1 and Tpm1.3, it was shown that the lack of N-terminal acetylation leads to an at least 30-fold lower actin affinity (Heald and Hitchcock-DeGregori, 1988; Hitchcock-DeGregori and Heald, 1987). Results available for Tpm3.$^{1}/_{3}$.2 and Tpm4.2 show that these cytoskeletal isoforms are almost exclusively acetylated in primary and transformed human fibroblasts and epithelial cells (Meiring et al., 2018). However, the precise impact of this post-translational modification on actin binding by cytoskeletal Tpm isoforms and the functional properties of A–Tpm cofilaments has remained unresolved. Further, N-terminal extensions consisting of one to three amino acid residues including Gly (Palm et al., 2003), Gly–Cys (Greenfield et al., 1994), Ala–Ser (Monteiro et al., 1994; Palm et al., 2003), Ala–Ala–Ser (Monteiro et al., 1994), Lys–Met–Thr (Heald and Hitchcock-DeGregori, 1988; Hitchcock-DeGregori and Heald, 1987), and Ala–Ser–Arg (Urbancikova and Hitchcock-DeGregori, 1994) have been shown to restore the high-affinity actin binding of the muscle-specific isoforms Tpm1.1 and Tpm1.3 with little or no interference with self-polymerization, myosin interactions and other regulatory functions (Hitchcock-DeGregori and Heald, 1987; Maytum et al., 2000; Monteiro et al., 1994). As such, these peptide extensions, but especially the Ala–Ser dipeptide, are now widely used as N-terminal acetylation mimics for the production of recombinant muscle-specific as well as cytoskeletal Tpm constructs (Coulton et al., 2006; Palm et al., 2003).

Considering the essential functions of actomyosin complexes in non-muscle cells and the almost complete association of cytoskeletal F-actin with Tpm cables (Meiring et al., 2018), it is of paramount importance to elucidate the contribution of Tpm cables to contractile processes by investigating the influence of their isoform composition, exon usage, and N-terminal acetylation (Arnesen et al., 2009; Silva and Martinho, 2015). Here, we describe how the activities of the cytoskeletal myosin isoforms Myo1C^0 (Adamek et al., 2008; Giese et al., 2020; Zattelman et al., 2017), NM-2A (Kovács et al., 2003; Müller et al., 2013), and myosin-5A (De La Cruz et al., 1999; Mehta et al., 1999; Rock et al., 2000), which exert distinct enzymatic properties and cellular functions, are regulated by different Tpm isoforms and how N-terminal Tpm acetylation influences the functional properties of these myosin isoforms. We show by biochemical analysis of reconstituted A–Tpm–M complexes that the motor activity of human Myo1C^0, NM-2A, and myosin-5A are each regulated in different ways by Tpm isoforms, and that N-terminal acetylation of Tpm alters this regulation to a significant extent and in a manner specific to each myosin isoform.

RESULTS

Expression, purification, and initial characterization of proteins for the *in vitro* reconstitution of physiological A–Tpm–M complexes

To characterize the functional properties of cytoskeletal A–Tpm cofilaments and their interactions with myosin motors, we produced and purified the human isoforms of β-actin, γ-actin, tail truncated versions of Myo1C isoform C^0 (Myo1C^0-ΔTH1), and heavy meromyosin (HMM)-like constructs of NM-2A and myosin-5A in active and soluble forms using the SF9/baculovirus system. In humans, alternative splicing of the *MYO 1C* gene leads to the production of three isoforms, which differ in the length of their N-terminal extensions (Ihnatovych et al., 2012; Nowak et al., 1997). Compared with Myo1C^0, the isoforms Myo1C^{16} and Myo1C^{35} contain 16 and 35 additional amino acids at their N-terminus. Typically, we obtained up to 3.5 mg of the cytoskeletal actin isoforms, 1.6-mg Myo1C^0-ΔTH1, 0.6 mg NM-2A-HMM, and 0.5 mg myosin-5A-HMM per 1 L of culture medium.

Human Tpm isoforms were produced in *Escherichia coli* BL21(DE3) for the non-acetylated isoforms and the acetylated isoforms in *E. coli* BL21(DE3) cells coproducing either the fission yeast NatA or NatB complex. The sequential induction of the appropriate Nat complex, followed by expression and repression of the respective Tpm isoform of interest, has been shown to result in near-complete N-terminal acetylation (Eastwood et al., 2017). Moreover, the presence of N-terminal acetylation was probed for isoforms derived from *TPM1* and *TPM2* using antibodies recognizing either the acetylated or non-acetylated Tpm N-terminus (Figure 2A). Both the non-acetylated and acetylated Tpm isoforms were purified to homogeneity in yields of 15–20 mg per liter. Previous work from our laboratory has shown significant differences in the ability of isoactins to bind and stimulate the enzymatic activity of human NM-2A, -2B, -2C, and myosin-7A. In the case of NM-2A and -2B, the interaction with either cytoplasmic actin isoform results in four-fold greater stimulation of myosin ATPase activity than was observed in the presence of α-skeletal muscle actin (Müller et al., 2013). Significant differences were also observed in initial control experiments performed for the interaction of human myosin-5A with the different isoactins. Accordingly, all subsequently described experiments using NM-2A and myosin-5A constructs were performed with cytoskeletal β-actin. The situation is different for Myo1C, where we observed no significant change in ATP turnover and motile activity upon exchange of the actin isoform (Figures S1A and S1B). Likewise, we observed comparable maximal inhibition of 40 ± 5% and IC_{50} values of 3.5 ± 0.3 μM for ATP turnover by acto-Myo1C^0-ΔTH1 in the presence of Tpm3.1 and AcTpm3.1. Therefore, all experiments involving Myo1C^0-ΔTH1 were performed using α-actin and non-acetylated Tpm isoforms.

To investigate the effects of exon usage 1a.2b in HMW–Tpm isoforms compared with 1b in LMW isoforms, as well as the importance of internal exon 6a compared to 6b, we performed cosedimentation tests with β-actin in combination with HMW–Tpm isoforms 1.6 and 2.1 or LMW isoforms 3.1 and 4.2. Myo1C motor functions were studied in detail in complex with Tpm1.7 and Tpm3.1 as *in vivo* and *in vitro* studies provide clear evidence for the role of Tpm1.7 and Tpm3.1 decorated actin cytoskeleton in the regulation of Myo1C localization at specific cell sites and motor functions (Kee et al., 2015; McIntosh et al., 2015; Pelham et al., 1996).

We observed values for half-maximal saturation of binding ($K_{50\%}$) in a narrow range between 1.3 and 2.0 μM with the HMW isoforms Tpm1.6 and Tpm2.1 and the LMW isoforms Tpm3.1, and Tpm4.2 (Figure 2C). Each of these isoforms is prominently associated with stress fibers in a variety of human cell types (Gateva et al., 2017). Tpm isoforms included in our study that are typically not associated with stress fibers such as Tpm1.8

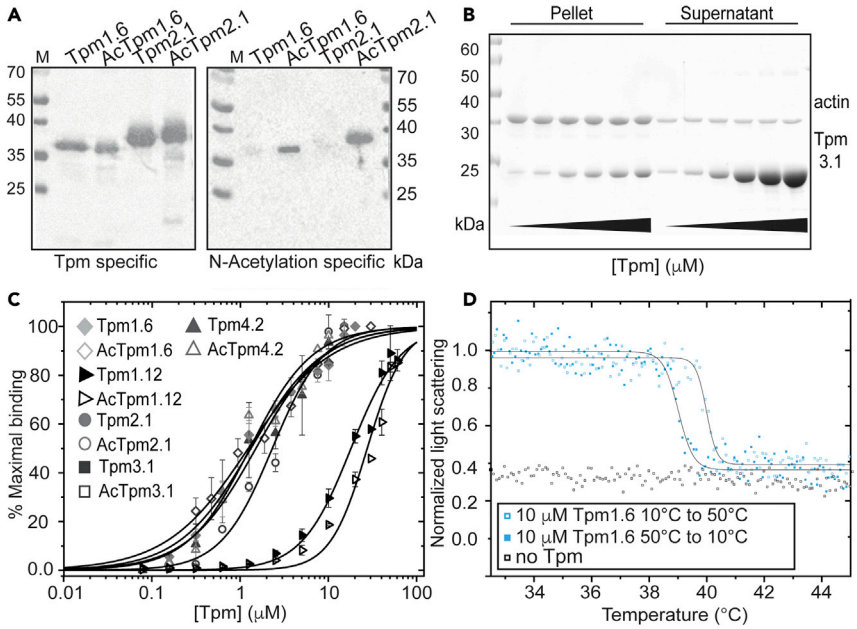

Figure 2. Interaction of distinct Tpm isoforms with actin and impact of the actin isoform used in functional assays

(A) Blot of non-acetylated and acetylated Tpm1.6 and Tpm2. 1 immunostained either with sheep polyclonal antibody Millipore AB5441 directed against isoforms containing a region encoded by exon 9d of *TPM1* or *TPM2* (left panel) or with rabbit polyclonal antibody D55Ac directed against the N-acetylated forms of gene products encoded by *TPM1* and *TPM2* (right panel).

(B) Coomassie gel showing the results of an A–Tpm3.1 cosedimentation assay. All samples contained 5-μM actin and increasing concentrations of Tpm3.1 (1–15 μM) in a buffer containing 20-mM MOPS pH 7.3, 50-mM KCl, 5-mM $MgCl_2$.

(C) Binding curves showing the interaction of F-actin with Tpm1.6, Tpm1.12, Tpm2.1, Tpm3.1, and Tpm4.2, in both the acetylated and non-acetylated forms. Fractional binding (Tpm/actin) was determined using cosedimentation assays as depicted in panel B. The results are shown normalized with 0 representing unbound and 1 fully bound Tpm isoforms. Data were fitted using the Hill equation. Apparent binding affinities are summarized in Table 1. Four independent experiments were carried out for each isoform, each with four individual measurements. Error bars represent standard deviations.

(D) Graph showing the temperature-induced dissociation (10–50 °C) and reassociation (50–10 °C) of A–Tpm1.6 cofilaments, monitored by recording the associated changes in light scattering intensity.

and Tpm1.12 have $K_{50\%}$ values that lie outside this narrow range. Approximately 10-fold higher and lower apparent binding affinities were observed with Tpm1.8 and Tpm1.12, respectively (Table 1).

Impact of N-terminal Tpm acetylation on interaction with filamentous actin

Following N-terminal acetylation, we observed only minor changes in the $K_{50\%}$ for filamentous β-actin, with increases in apparent binding affinity for the N-acetylated forms from 1.32 to 1.23 μM for Tpm1.6, 1.50 to 1.15 μM for Tpm3.1, and 1.99 to 1.33 μM for Tpm4.2. The opposite effect was observed upon acetylation for Tpm1.12 and Tpm2.1, resulting in a decrease in apparent binding affinity from 18.2 to 28.8 μM and 1.73 to 2.29 μM, respectively (Figures 2C and Table 1). At least in the absence of other actin-binding proteins, our results support the view that there exists no direct relationship between the F-actin binding affinities of cytoskeletal Tpm isoforms and molecular weight (Carman et al., 2021; Janco et al., 2016; Moraczewska et al., 1999; Ngo et al., 2016). Our results show in addition that N-terminal acetylation has only a minor impact on the actin affinity of cytoskeletal Tpm isoforms, again without a clear correlation to size.

Next, we investigated whether the thermal stability of A–Tpm cofilaments is altered by N-terminal acetylation. In agreement with previous data obtained using smooth muscle isoforms (Levitsky et al., 2000), we show that the dissociation of cytoskeletal Tpm isoforms from filamentous β-actin is reversible and shows pronounced hysteresis, with dissociation occurring at higher temperatures than reassociation (Figure 2D). A comparison of T_{diss} for non-acetylated and acetylated Tpm1.6, Tpm2.1, Tpm3.1, and Tpm4.2 revealed significant isoform-specific differences in dissociation properties (Figures 3A–3D, Table 1). Specifically,

Table 1. Apparent Tpm binding affinities ($K_{50\%}$) and temperature stability of A–Tpm cofilaments

Tpm Isoform	Exon usage MW	$K_{50\%}$ [μM][a]	T_{diss} [°C][b]	T_{ass} [°C][b]	ΔT [°C]
Tpm1.6	1a.2b.6b.9d 32.7 kDa	1.32 ± 0.12	41.2 ± 0.6	39.0 ± 0.4	2.2 ± 0.6
AcTpm1.6	1a.2b.6b.9d 32.7 kDa	1.23 ± 0.14	39.6 ± 0.5	39.3 ± 0.4	0.3 ± 0.5
Tpm1.8	1b.–.6b.9d 28.6 kDa	0.1 ± 0.03	41.6 ± 0.1	39.0 ± 0.2	2.6 ± 0.2
Tpm1.12	1b.–.6b.9c 28.5 kDa	18.2 ± 1.5	ND	ND	ND
AcTpm1.12	1b.–.6b.9c 28.5 kDa	28.8 ± 1.9	47.5 ± 0.1[c]	ND	ND
Tpm2.1	1a.2b.6a.9d 32.9 kDa	1.73 ± 0.19	38.0 ± 0.1	37.4 ± 0.2	0.6 ± 0.2
AcTpm2.1	1a.2b.6a.9d 32.9 kDa	2.29 ± 0.23	37.6 ± 0.2	37.2 ± 0.3	0.4 ± 0.3
Tpm3.1	1b.–.6a.9d 29.0 kDa	1.50 ± 0.19	35.6 ± 0.4	29.8 ± 0.1	5.8 ± 0.4
AcTpm3.1	1b.–.6a.9d 29.0 kDa	1.15 ± 0.15	44.7 ± 0.7	43.6 ± 0.4	1.1 ± 0.7
Tpm4.2	1b.–.6b.9d 28.5 kDa	1.99 ± 0.83	36.5 ± 0.5	31.2 ± 0.3	5.3 ± 0.5
AcTpm4.2	1b.–.6b.9d 28.5 kDa	1.33 ± 0.41	>50	ND	ND

[a]Experiments were performed in cosedimentation buffer containing 20-mM MOPS pH 7.0, 100-mM KCl, and 5-mM $MgCl_2$. The β-actin concentration was set to 5 μM, Tpm was titrated from 0.125 to 20 μM for all constructs with the exception of Tpm1.12, where the titration was performed over the range 0.125–40 μM $K_{50\%}$ values were calculated after fitting the sigmoidal binding curves using the Hill equation. At least four independent experiments were performed with each Tpm isoform.
[b]Experiments were performed in light-scattering buffer containing 20-mM potassium phosphate pH 7.4 and 50-mM NaCl. The β-actin concentration was set to 5 μM and the Tpm concentration to 10 μM. Tdiss and Tass are the temperatures at which a 50% change in the intensity of the light scattering signal occurs. At least three independent experiments, each involving three to five individual measurements, were performed with each isoform. The results correspond to the mean value ±SD.
[c]Value taken from Marchenko et al. (2021) for a recombinant Tpm1.12 with an Ala–Ser N-terminal extension to mimic N-terminal acetylation. Experimental conditions: 10-μM phalloidin-stabilized α-actin and 120-μM Ala–Ser–Tpm1.12 in 30-mM HEPES, 100-mM NaCl, 2-mM DTT, pH7.3.

in the absence of N-terminal acetylation, the HMW isoforms Tpm1.6 and Tpm2.1 display higher T_{diss} values of 41.2° and 38.0 °C than the LMW isoforms Tpm3.1 and Tpm4.2 with T_{diss} values of 35.6° and 36.5 °C. In the case of the HMW isoforms, N-terminal acetylation leads to a slight reduction of T_{diss}. In contrast, the LMW isoforms show marked stabilization of their cofilaments with F-actin by 9°C or more after N-terminal acetylation. In the case of Tpm4.2, N-terminal acetylation shifts the light scattering signal into the range where denaturation of F-actin starts to occur, the observed processes become irreversible, and dissociation cannot be fully resolved (Figures 3D and Table 1). In line with previous studies (Levitsky et al., 2000), we observed that the T_{diss} values measured for the different acetylated and non-acetylated isoforms depend strongly on Tpm concentration. Secondary plots of T_{diss} against the total Tpm concentration are well described by hyperbolas. N-terminal acetylation of Tpm 1.6 resulted in small increases in T_{diss} over the entire concentration range. A much stronger stabilization of cofilaments was observed after N-terminal acetylation of Tpm3.1, evident from a marked leftward shift and an approximately 10 °C higher plateau value of the hyperbola (Figures 3E and 3F).

Modulation of actin-activated ATPase and motor activity of myosin-1C^0 by cytoskeletal Tpm isoforms

The actin-activated steady-state ATPase activities of Myo1C^0-ΔTH1 were determined with 10-μM A–Tpm cofilaments composed of α-actin and non-acetylated LMW isoforms Tpm3.1, Tpm4.2, or HMW isoforms Tpm1.6, Tpm1.7. Marked reductions in ATP turnover of Myo1C^0-ΔTH1 were observed in the presence of all Tpm isoforms tested (Figure 4A). It should be noted that the ATPase rates reported in Table 2 refer to values obtained at a sub-saturating concentration of 10-μM A–Tpm cofilaments and thus cannot be directly compared with the values obtained at saturating concentrations of bare F-actin and Tpm cofilaments. The actin-activated steady-state ATPase activities of Myo1C^0-ΔTH1 in the absence and presence of HMW isoform Tpm1.7 or LMW isoform Tpm3.1 were determined at actin concentrations ranging from 0 to 50 μM. Under both conditions, we observed a reduction in maximum ATP turnover of approximately 33% for Myo1C^0-ΔTH1 (Table 2). We used stopped-flow kinetics to determine the impact of HMW Tpm1.7 and LMW Tpm3.1 on the binding of Myo1C^0-ΔTH1 to F-actin in the absence of nucleotide, ATP-induced dissociation of Myo1C^0-ΔTH1 from F-actin, ADP affinity of acto-Myo1C^0-ΔTH1, and the release of the hydrolysis products phosphate and ADP. The results of these measurements are summarized in Table 3. They show a significant reduction in the rate constant for phosphate release (k_{+4}) from 0.09 ± 0.01 s^{-1} in the presence of bare F-actin

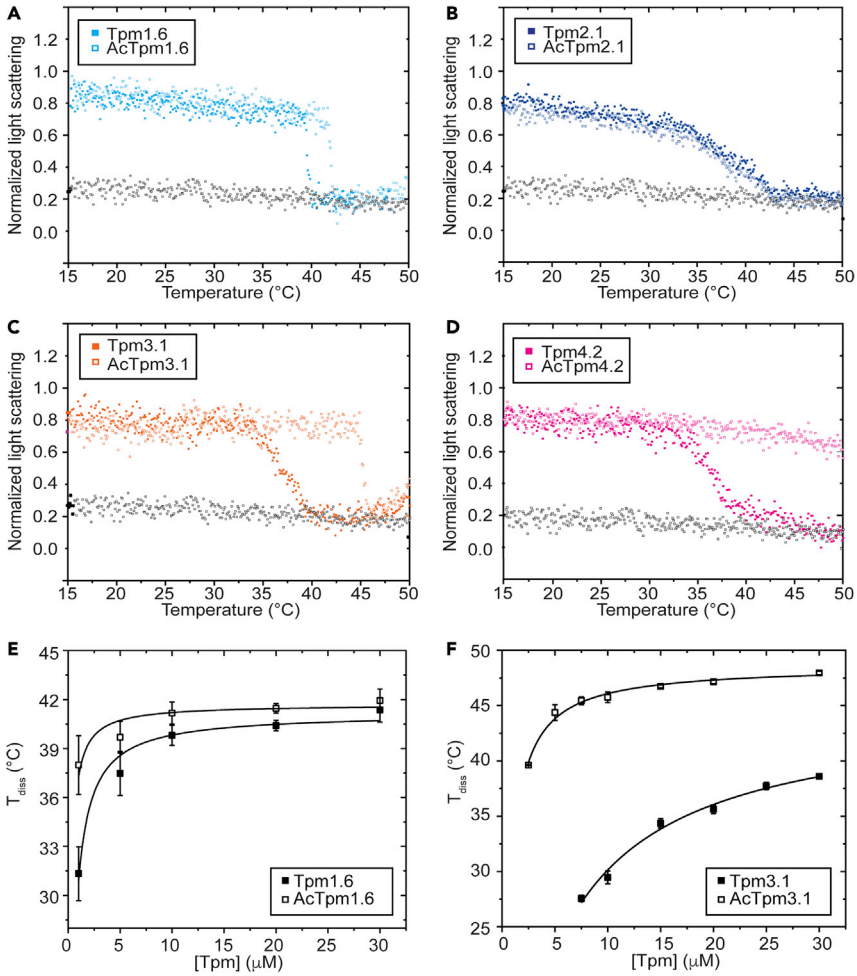

Figure 3. Acetylation of Tpm results in isoform specific changes in the temperature-induced dissociation of the cofilaments with F-actin as indicated by the decrease in light scattering

(A) N-terminal acetylation of Tpm1.6 at 10-μM Tpm results in a shift of 1.6 °C to higher temperatures.

(B) N-terminal acetylation of Tpm2.1 does not affect the dissociation dynamics and T_{diss}.

(C) N-terminal acetylation exerts a significantly higher impact on the T_{diss} of the LMW Tpm isoforms. Acetylation of Tpm3.1 increases T_{diss} at 10 μM by about 9 °C.

(D) N-terminal acetylation of Tpm4.2 leads to an even greater increase in T_{diss}, into a range where denaturation of actin starts to interfere with the dissociation associated light scattering signal.

(E and F) Secondary plots showing the dependence of T_{diss} on [Tpm1.6] and [Tpm3.1] in the absence and presence of N-terminal acetylation. Three independent experiments for each data point were performed with each isoform. Symbols represent mean values ±SD.

to 0.07 ± 0.01 s^{-1} in the presence of cofilaments containing either Tpm1.7 or Tpm3.1. We have previously shown that in the presence of bare F-actin k_{cat}, the maximum value of ATP turnover in the presence of saturating actin concentrations, is reduced from ~0.37 s^{-1} at 37 °C to 0.09 ± 0.02 s^{-1} at 20 °C (Giese et al., 2020). Thus, in the absence and presence of Tpm isoforms, the observed differences between the rate limiting step k_{+4} and k_{cat} are primarily owing to the different temperatures at which the transient and steady-state kinetics experiments were performed. The impact of the Tpm isoforms on the rate of ADP release from Myo1C^0-ΔTH1 was determined by ATP-induced dissociation of the actomyosin complex (Geeves, 1989). The active sites of 0.5-μM Myo1C^0-ΔTH1 were saturated with 20-μM ADP, so that ATP binding is rate-limited by the slow dissociation of ADP. The transients were best fitted with a single exponential function yielding rate constants for ADP release (k_{+5}) that are 30 and 34% slower for cofilaments containing Tpm1.7 (1.11 ± 0.09 s^{-1}) and Tpm3.1 (1.05 ± 0.05 s^{-1}) than the rate constant obtained with bare F-actin (1.59 ± 0.07 s^{-1}). Finally, measurements of the ATP-induced dissociation of pyrene-labeled acto-Myo1C^0-ΔTH1 revealed a

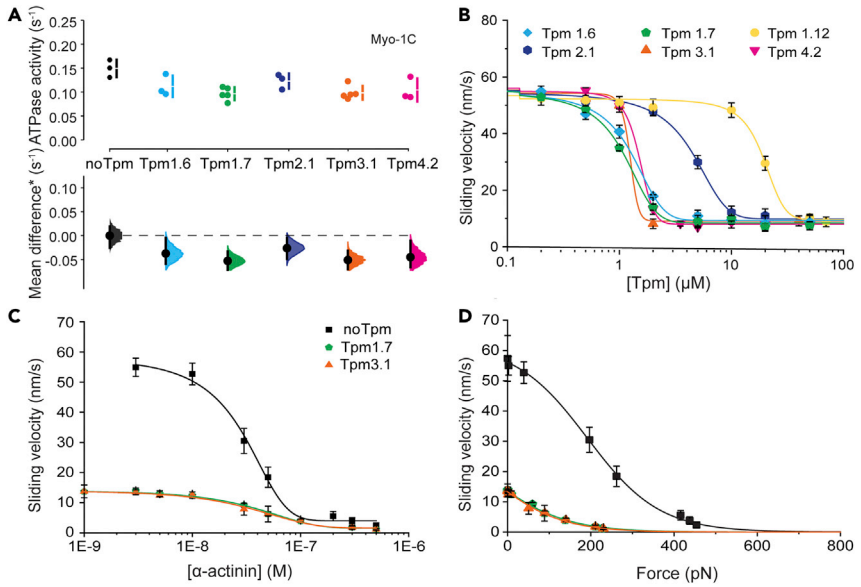

Figure 4. Tpm-dependent changes in the kinetic and functional behavior of Myo1C^0-ΔTH1

(A) Cumming estimation plot showing the results of ATPase assays performed with 0.1-μM phosphorylated Myo-1C in the presence of filamentous β-actin (10 μM) or A–Tpm cofilaments (10 μM). ATPase assays were performed at 37 °C and results are given as ATP turnover per myosin motor. At least three independent experiments were performed for each experimental condition. The upper part of the Cumming estimation plot shows the results of individual measurements as a swarmplot with mean ± SD represented by a broken line right next to the data points. The lower part shows effect sizes as bootstrapped 95% confidence intervals (CI) with a separate, aligned axis. If the 95% CI contains the null value and the vertical bar is crossing the horizontal line of null effect, the combined results are considered not statistically different.

(B) Dose-response curves for the inhibition of the motile activity of Myo-1C by different cytoskeletal Tpm isoforms. Half-maximal inhibitory concentrations (IC_{50}) correspond to Tpm1.7 (1.0 ± 0.1 μM), Tpm1.6 (1.2 ± 0.2 μM), Tpm3.1 (1.3 ± 0.9 μM), Tpm2.1 (4.2 ± 0.4 μM), and Tpm4.2 (1.5 ± 0.1 μM). Tpm1.12 (19.3 ± 1.1 μM). Sliding velocities were measured at 37 °C. (C) Tpm isoform-specific differences in the load-dependence of Myo1C-driven movement of A–Tpm cofilaments were examined using the frictional load assay (Greenberg and Moore, 2010). External loads applied by the addition of increasing concentrations of α-actinin reduce the filament sliding velocity of bare F-actin and cofilaments containing Tpm1.7 or Tpm3.1 to different extents.

(D) The observed load-dependent changes in sliding velocities are best described by a tension-sensing mechanism that includes a force-dependent and a force-independent transition.

(B–D) Values from at least three independent experiments are shown as mean and SD .

significant change in the equilibrium constant for isomerization of the nucleotide-binding pocket K_α indicating a shift toward greater occupancy of states with closed nucleotide binding pocket in the presence of cofilaments containing Tpm1.7 or Tpm3.1.

To determine the influence of A–Tpm cofilaments on myosin-1C motor function, we performed *in vitro* motility assays. No motile activity was detectable on Myo1C^0-ΔTH1-decorated surfaces, when bare actin filaments were replaced with A–Tpm cofilaments under the standard conditions of the *in vitro* motility assay. Titrations of the Myo1C^0-ΔTH1surface density showed that the minimum motor density to achieve a stable plateau value for continuous directional movement increased from 900 motors μm^{-2} with bare F-actin to >4,000 motors μm^{-2} in the presence of A–Tpm cofilaments (Figure S2). Compared with the plateau value of 52.1 ± 4.9 nm s^{-1} obtained for filament sliding velocity with bare F-actin on lawns of Myo1C^0-ΔTH1, approximately 5.5-fold slower values were observed in the presence of Tpm1.6, Tpm1.7, Tpm1.12, Tpm2.1, Tpm3.1, and Tpm4.2 (Table 2). Based on results obtained with class-2 myosins (Greene and Eisenberg, 1980; Ngo et al., 2016), we expected the cytoskeletal Tpm isoforms and Myo1C^0 to mutually strengthen each other's affinity for F-actin in the presence of ATP. With NM-2B, we had observed a change in the $K_{50\%}$ for F-actin binding by Tpm1.12 from ≥40 μM to <1 μM (12). However, when we replaced NM-2B with Myo1C^0, a much smaller increase in the apparent actin affinity of Tpm1.12 ($K_{50\%}$ = 19.3 ± 1.1 μM) was recorded. The reduced mutual cooperative enhancement of actin binding by the cytoskeletal Tpm isoforms and Myo1C^0 is clearly evident in the dose-response curves for inhibition of Myo1C^0-supported motile

Table 2. Impact of changes in Tpm isoform on ATP turnover and unloaded velocity

A–Tpm	Sliding velocity (nm s^{-1})	ATP turnover (s^{-1})	K_{app} (μM)	k_{cat}/K_{app} ($\mu M^{-1}s^{-1}$)
Myo1C^0-ΔTH1 (measured at 37 °C)				
No Tpm	52.1 ± 4.9	0.17 ± 0.02[b] 0.38 ± 0.02[a]	12.42 ± 0.75	0.024 ± 0.001
Tpm1.6	11.5 ± 2.1	0.11 ± 0.03[b]	ND	ND
Tpm1.7	10.5 ± 4.9	0.12 ± 0.02[b] 0.24 ± 0.02[a]	11.03 ± 0.60	0.015 ± 0.001
Tpm3.1	11.5 ± 1.7	0.11 ± 0.02[b] 0.25 ± 0.02[a]	12.03 ± 0.85	0.016 ± 0.001
Tpm2.1	11.8 ± 2.3	0.13 ± 0.02[b]	ND	ND
Tpm4.2	10.4 ± 2.1	0.11 ± 0.03[b]	ND	ND
NM-2A-HMM (measured at 30 °C)				
No Tpm	103.2 ± 8.9	0.26 ± 0.02[a]	27.6 ± 6.7	0.0081 ± 0.0010
Tpm1.6	116.9 ± 19.5	0.35 ± 0.02[a]	27.8 ± 4.6	0.0124 ± 0.0015
AcTpm1.6	157.9 ± 21.3	0.31 ± 0.01[a]	17.7 ± 2.3	0.0174 ± 0.0015
Tpm2.1	115.9 ± 8.6	0.40 ± 0.04[a]	37.8 ± 11.1	0.0102 ± 0.0015
AcTpm2.1	124.6 ± 13.8	0.41 ± 0.03[a]	40.9 ± 7.3	0.0099 ± 0.0010
Tpm3.1	168.6 ± 15.2	0.64 ± 0.07[a]	19.6 ± 6.3	0.0291 ± 0.0020
AcTpm3.1	166.9 ± 10.1	0.48 ± 0.04[a]	26.6 ± 5.5	0.0180 ± 0.0010
Tpm4.2	98.5 ± 11.6	0.37 ± 0.02[a]	26.2 ± 5.6	0.0112 ± 0.0010
AcTpm4.2	145.7 ± 20.1	0.61 ± 0.06[a]	26.1 ± 6.1	0.0234 ± 0.0015
Myosin-5A-HMM (measured at 30 °C)				
No Tpm	376.8 ± 20.7	1.05 ± 0.14[b]	ND	ND
Tpm1.6	272.1 ± 36.2	0.71 ± 0.09[b]	ND	ND
AcTpm1.6	262.9 ± 46.1	0.76 ± 0.10[b]	ND	ND
Tpm1.12	423.0 ± 8.1	1.02 ± 0.08[c]	ND	ND
AcTpm1.12	397.9 ± 5.5	1.00 ± 0.11[c]	ND	ND
Tpm2.1	247.2 ± 22.5	0.64 ± 0.14[b]	ND	ND
AcTpm2.1	277.2 ± 20.9	0.60 ± 0.06[b]	ND	ND
Tpm3.1	256.7 ± 29.0	0.76 ± 0.07[b]	ND	ND
AcTpm3.1	245.8 ± 29.0	0.74 ± 0.06[b]	ND	ND
Tpm4.2	259.4 ± 18.1	0.61 ± 0.10[b]	ND	ND
AcTpm4.2	247.1 ± 7.3	0.61 ± 0.13[b]	ND	ND

[a]The actin-activated ATPase activities of NM-2A-HMM and Myo1C^0-ΔTH1 were measured as a function of [A] or [A–Tpm]. Values for k_{cat} and K_{app} were calculated by fitting the data to the Michaelis–Menten equation. R^2 was within the range of 0.92–0.99. At least six independent ATPase assays were performed, each involving three to five individual measurements.
[b]Actin-activated ATPase activity measured in the presence of 20-μM F-actin and 15-μM Tpm, except the low-affinity Tpm1.12, where 30 μM were used. Control measurements were performed with 20-μM F-actin in the absence of Tpm. At least four independent experiments were performed, each involving three to five individual measurements. Results correspond to the mean value ±SD.
[c]Actin-activated ATPase activity measured in the presence of 20-μM F-actin and 30-μM Tpm. Control measurements were performed with 20-μM F-actin in the absence of Tpm. At least four independent experiments were performed, each involving three to five individual measurements. Results correspond to the mean value ±SD.

activity by the various cytoskeletal Tpm isoforms (Figure 4B). Tpm2.1 showed a similar two-fold change in $K_{50\%}$ in the presence of Myo1C^0. Smaller changes were recorded for cofilaments containing Tpm3.1 and Tpm4.2 in the presence of Myo1C^0, with increases in $K_{50\%}$ of 13 and 25%, respectively (Table 1).

To analyze the influence of the distinct Tpm isoforms on Myo1C-driven force development, we determined the ability of Myo1C^0-ΔTH1 to translocate A–Tpm cofilaments in the presence of an external load using frictional loading experiments (Greenberg and Moore, 2010). Binding of surface-attached α-actinin to A–Tpm

Table 3. Impact of changes in Tpm isoform on the transient kinetic parameters for acto-Myo1C^0

	Signal and measured parameter	No Tpm	Tpm1.7	Tpm3.1
Active site isomerization				
K_α	Pyrene–actin; A_{fast}/A_{slow}	0.90 ± 0.03	0.76 ± 0.06	0.73 ± 0.06
$k_{+\alpha}$ (s^{-1}) (20 °C)	Pyrene–actin, $k_{max,\ slow}$	4.1 ± 0.2	3.2 ± 0.2	3.2 ± 0.2
(37 °C)		9.7 ± 0.4	10.7 ± 0.8	9.9 ± 0.3
$k_{-\alpha}$ (s^{-1})	$k_{+\alpha}/K_\alpha$ (calc.)	4.56 ± 0.37	4.21 ± 0.46	4.38 ± 0.63
ATP-binding to actomyosin				
$1/K_1$ (μM)				
k_{+2} (s^{-1}) (20 °C)	Pyrene–actin, $K_{0.5,fast}$	154 ± 31	136 ± 14	134 ± 19
(37 °C)	Pyrene–actin, $k_{max,\ fast}$	37.1 ± 1.6	23.0 ± 0.5	22.3 ± 0.7
K_1k_{+2} ($\mu M^{-1}\ s^{-1}$) [a]		69.5 ± 1.9	70.1 ± 1.8	76.8 ± 1.7
	Pyrene–actin, initial slope	0.16 ± 0.01	0.12 ± 0.01	0.12 ± 0.01
Actomyosin binding (in absence of nucleotides)				
k_{+A} ($\mu M^{-1}\ s^{-1}$) [b]	Pyrene–actin, slope	1.46 ± 0.07	1.33 ± 0.03	1.36 ± 0.04
k_{-A} (s^{-1})	Pyrene–actin, k_{obs}	0.019 ± 0.001	0.025 ± 0.001	0.025 ± 0.001
K_A (nM)	k_{-A}/k_{+A} (calc.)	13.7 ± 0.1	19.6 ± 0.2	18.4 ± 0.3
Phosphate release				
k_{obs} (s^{-1}) [c]	MDCC–PBP	0.021 ± 0.001	0.015 ± 0.001	0.29 ± 0.15
k_{+4} (s^{-1})	(calc.)	0.09 ± 0.01	0.07 ± 0.01	0.05 ± 0.01
ADP binding of actomyosin				
K_5 (μM) [d]	Pyrene–actin, A_{slow}/A_{total}	0.46 ± 0.08	0.32 ± 0.17	0.29 ± 0.15
k_{+5} (s^{-1}) (20 °C)	Pyrene–actin, $k_{min,\ slow}$	1.59 ± 0.07	0.32 ± 0.17	1.05 ± 0.05
(37 °C)		7.8 ± 0.1	7.3 ± 0.3	7.1 ± 0.2
k_{-5} ($\mu M^{-1}s^{-1}$)	k_{+5}/K_5 (calc.)	3.45 ± 0.75	3.47 ± 2.12	3.62 ± 2.05

25 -mM HEPES pH 7.5, 50-mM KCl, 5-mM $MgCl_2$, 0.5-mM DTT at 20°C, unless otherwise specified
[a]derived from the initial slope of the plot $k_{obs,\ fast}$ versus [ATP].
[b]derived from the slope of the plot k_{obs} versus [actin].
[c]in the presence of 5-μM F-actin at 20°C, values for k_{+4} in the presence of saturating [actin] and at 20°C are estimated on the basis of the steady-state ATPase measurements.
[d]derived from the fit A_{slow}/A_{total} = [ADP]/(K_5 + [ADP]).

cofilaments leads to a reduction in the filament sliding velocity as the external load increases with the concentration α-actinin and impedes the driving force of myosin (Figure 4C). We have previously observed that the load-dependent changes in the sliding velocities of Myo1C^0–ΔTH1 are best described by a tension-sensing mechanism that includes a force-dependent and a force-independent transition (Giese et al., 2020). The resulting force-velocity dependences (Figure 4D) indicate a marked reduction in motive power generation in the presence of actin cofilaments containing Tpm1.7 or Tpm3.1.

Modulation of actin-activated ATPase and motor activity of non-muscle myosin-2A and myosin-5A by non-acetylated cytoskeletal Tpm isoforms

The observed maximum actin-activated ATPase activity of NM-2A with bare filamentous β-actin (k_{cat} = 0.26 ± 0.02 s^{-1}) is in good agreement with published data (Hundt et al., 2016; Kovács et al., 2003). Functional assays performed with NM-2A in the presence of saturating concentrations of non-acetylated HMW tropomyosin isoforms Tpm1.6 and Tpm2.1 and LMW isoforms Tpm3.1 and Tpm4.2 show isoform-specific variations in catalytic activity. The strongest effect was observed for Tpm3.1, with a 2.5-fold increase in k_{cat} and 63% faster velocity compared with bare F-actin. Cofilaments containing Tpm2.1 showed a 1.5-fold increase in k_{cat} and a 12% faster velocity. In the case of Tpm1.6 and Tpm4.2, we observed a 34 and 42% increase in k_{cat} together with smaller changes in velocity, which are within the margin of error of our assay (Figures 5A and 5B; Table 2).

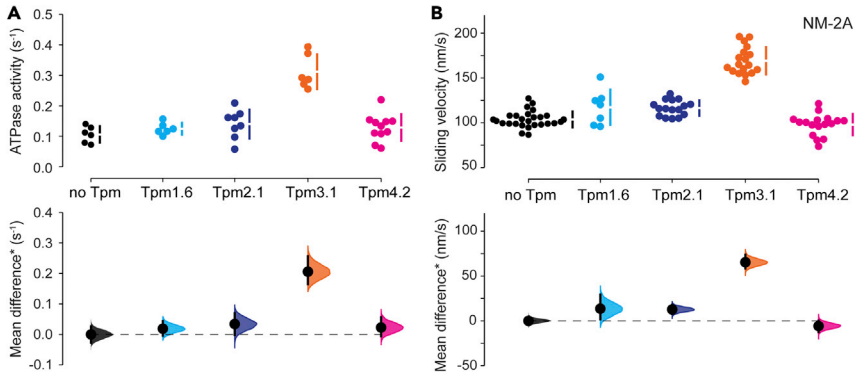

Figure 5. Tpm-dependent changes in the kinetic and functional behavior of NM-2A

(A) Cumming estimation plot showing the results of ATPase assays performed with 0.5-μM phosphorylated NM-2A-HMM in the presence of filamentous β-actin (20 μM) or A–Tpm cofilaments (20 μM). Six or more independent experiments, each involving at least three individual measurements, were performed for each experimental condition.

(B) Cumming estimation plot showing the results of *in vitro* motility assays performed with F-actin or A–Tpm cofilaments on surfaces decorated with phosphorylated NM-2A-HMM. Seven or more independent experiments, each involving at least five technical replicates with >100 trajectories, were performed for each experimental condition. All assays were performed at 30 °C. The results of the individual measurements are shown as a swarmplot with mean ± standard deviation (SD) represented by a broken line. Effect sizes are shown as bootstrapped 95% confidence intervals (CI) on a separate, aligned axis. If the 95% CI contains the null value and the vertical bar is crossing the horizontal line of null effect, the combined results are considered not statistically different.

Assays performed with myosin-5A in the presence of saturating concentrations of non-acetylated Tpm1.6, Tpm2.1, Tpm3.1, and Tpm4.2 show reductions in actin-activated ATP turnover and sliding velocities ranging from 28 to 42% compared with bare F-actin (Figures 6A and 6B; Table 2). In contrast, cofilaments containing Tpm1.12 move approximately 12% faster than bare F-actin at a myosin-5A-HMM surface density corresponding to approximately 18 double-headed motor molecules per μm^2. ATP turnover by myosin-5A was not significantly affected by cofilaments containing Tpm1.12. With respect to the run length of filaments, we observed a significant reduction for cofilaments containing Tpm1.12 and a significant increase for those containing Tpm4.2. The run length of cofilaments containing Tpm1.6, Tpm2.1, or Tpm3.1 was unchanged compared with bare filamentous β-actin (Figure S3). Similar protection of filaments from fragmentation was observed for all Tpm isoforms tested.

Impact of N-terminal Tpm acetylation on actin-activated ATPase and motor activity of NM-2A and myosin-5A

For the HMW isoforms Tpm1.6 and Tpm2.1, only minor differences in the k_{cat} of NM-2A were observed between the acetylated and non–acetylated forms of the proteins. The observed changes in the concentration required for half-maximal activation of ATP turnover (K_{app}) are within the margin of error of our assay (Figures 7A and 7B). Larger opposing effects were observed for NM-2A in the presence of saturating concentrations of A–Tpm cofilaments containing either the acetylated or non-acetylated forms of LMW Tpm3.1 and Tpm4.2. Cofilaments containing Tpm3.1 show a 2.5-fold increase in k_{cat} (0.26 s^{-1} versus 0.64 s^{-1}), whereas K_{app} is reduced 1.4-fold and k_{cat}/K_{app} is more than 3.6-fold increased in the presence of Tpm3.1. These are the strongest effects observed for a non-acetylated Tpm isoform (Figure 7C). N-terminal acetylation of Tpm3.1 reduces the increase in k_{cat}/K_{app} to 2.2-fold, together with corresponding changes in k_{cat} and K_{app}. In the case of Tpm4.2, N-terminal acetylation has the opposite effect than that observed with Tpm3.1. The calculated k_{cat} is increased 1.6-fold for AcTpm4.2 from 0.37 to 0.61 s^{-1} and k_{cat}/K_{app} increases 2.1-fold from 1.12×10^{-2} to 2.34×10^{-2} $\mu M^{-1}s^{-1}$ in the presence of AcTpm4.2 (Figure 7D).

AcTpm1.6, AcTpm2.1, AcTpm3.1, and AcTpm4.2 containing cofilaments move approximately 53, 21, 63, and 43% faster on lawns of NM-2A than bare F-actin (Figure 7E). Whereas k_{cat} is reduced by 25% in the presence of AcTpm3.1 compared to Tpm3.1, both Tpm3.1 and AcTpm3.1 containing cofilaments move on lawns of NM-2A with the same velocity and approximately 63% faster than bare F-actin. With this exception

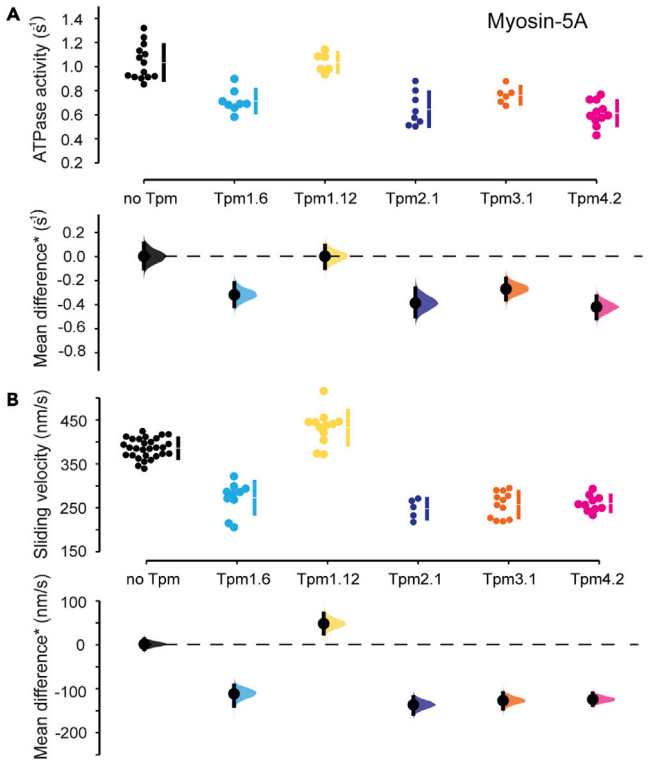

Figure 6. Tpm-dependent changes in actin-activated ATP turnover and functional behavior of myosin-5A

(A) Cumming estimation plot showing the results of ATPase assays performed with 0.1-μM myosin-5A-HMM in the presence of filamentous β-actin (20 μM) or A–Tpm cofilaments (20 μM). At least six independent experiments, each involving at least four technical repeats, were performed for each experimental condition.

(B) Cumming estimation plot showing the results of *in vitro* motility assays performed with F-actin or A–Tpm cofilaments on surfaces decorated with myosin-5A-HMM. Five or more independent experiments, each involving at least four technical replicates with >100 trajectories, were performed for each experimental condition. All assays were performed at 30 °C. The results of the individual measurements are shown as a swarmplot with mean ± standard deviation (SD) represented by a broken line. Effect sizes are shown as bootstrapped 95% confidence intervals (CI) on a separate, aligned axis. If the 95% CI contains the null value and the vertical bar is crossing the horizontal line of null effect, the combined results are considered not statistically different.

all other cofilaments containing AcTpm isoforms move faster than cofilaments containing the non-acetylated Tpm isoforms. In the case of Tpm2.1 and Tpm4.2, the changes in motor activity observed upon N-terminal acetylation correspond to the trend observed in ATP turnover measurements. Following N-terminal acetylation, similar increases in both parameters were observed for Tpm2.1 (<8%) and Tpm4.2 (>40%). In contrast, N-terminal acetylation of Tpm1.6 results in a 35% increase in sliding velocity but a 11% decrease in k_{cat} (Figure 7; Table 2).

In the case of myosin-5A, the differences in unloaded velocity, event frequency, and run length between acetylated and nonacetylated Tpm isoforms are mostly within the margin of error, with the following exceptions. Cofilaments containing Tpm1.12 move significantly faster on lawns of myosin-5A-HMM than bare filamentous β-actin and cofilaments containing AcTpm1.12 (Figure 8; Table 2). The percentage of filaments showing unidirectional uniform motion on lawns of myosin-5A-HMM was equal and higher than 98% for bare filaments and all cofilaments studied. Similar protection of filaments from fragmentation was observed for the acetylated and nonacetylated Tpm isoforms. The run length of cofilaments containing AcTpm1.6 or AcTpm3.1 was unchanged relative to bare filamentous β-actin and cofilaments containing the nonacetylated Tpm isoforms. Cofilaments containing Tpm2.1 showed a small but significant increase in run length that was not observed for AcTpm2.1. The run lengths of cofilaments containing Tpm4.2 and AcTpm4.2 were 8 and 12% longer, whereas those of cofilaments containing Tpm1.12 or AcTpm1.12 were approximately 15 and 20% shorter, respectively (Figure S3).

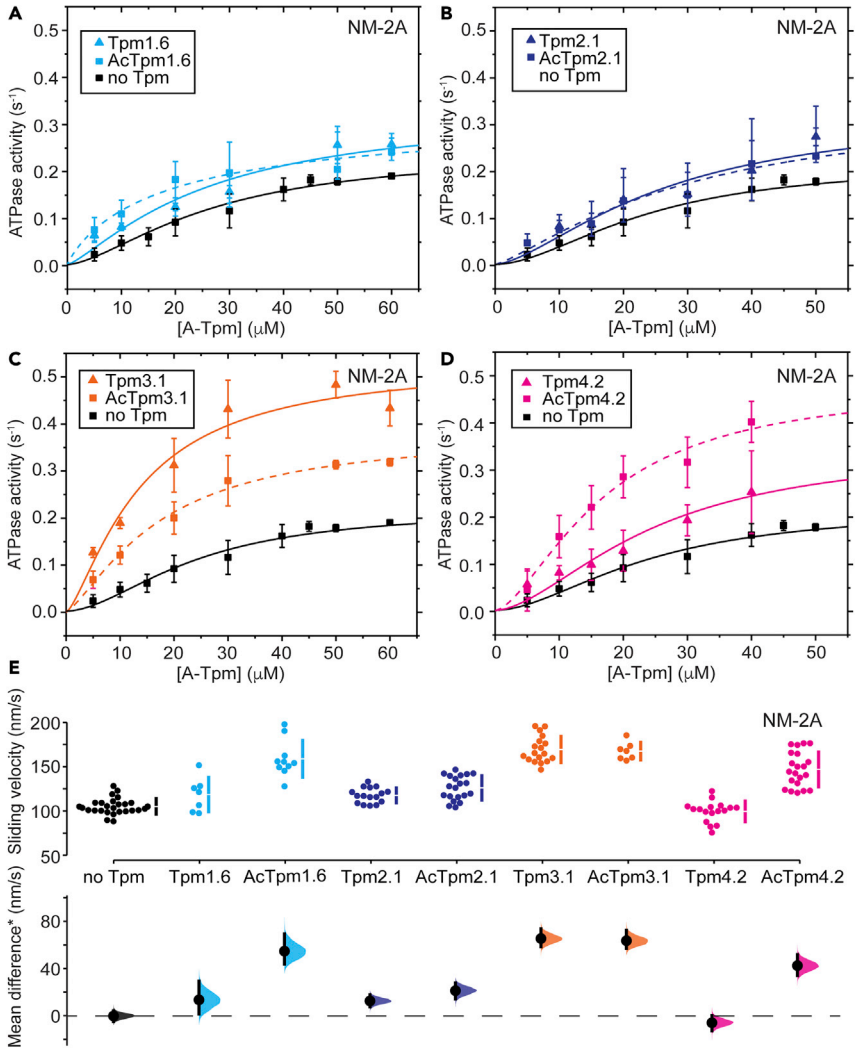

Figure 7. N-terminal acetylation of Tpm-dependent changes in the kinetic and functional behavior of NM-2A

(A–D) The actin-activated ATPase activity of NM-2A-HMM was measured with increasing [A–Tpm]. The assays were performed with 0.5-μM phosphorylated NM-2A-HMM at 30 °C. Six or more independent experiments, each involving at least three individual measurements, were performed with each isoform. Error bars represent standard deviations.

(E) Cumming estimation plot showing the influence of the different Tpm isoforms and their acetylated form on the sliding velocity of NM-2A. Seven or more independent experiments, each involving at least five technical replicates with >100 trajectories, were performed with each isoform. The results of the individual measurements are shown as a swarmplot with mean ± standard deviation (SD) represented by a broken line. Effect sizes are shown as bootstrapped 95% confidence intervals (CI) on a separate, aligned axis. If the 95% CI contains the null value and the vertical bar is crossing the horizontal line of null effect, the combined results are considered not statistically different.

DISCUSSION

Actin–Tpm interactions

Myosin–induced contraction has long been studied in skeletal and cardiac muscle, where thin actin filaments move along thick myosin filaments and actomyosin-based motility is regulated by Tpm-dependent cooperative on-off switching, which is mediated by the binding of Ca^{2+} to the troponin-C subunit of the troponin–Tpm complex on thin filaments (Greaseri and Gergely, 1971). The binding of Tpm to F-actin has been extensively characterized for the muscle isoforms and more recently also for individual cytoskeletal Tpm isoforms (Marchenko et al., 2021; Maytum et al., 2001; Pathan-Chhatbar et al., 2018; Schmidt et al., 2015). Emerging experimental results and molecular dynamics simulations support a form–function relationship that has been referred to as Gestalt-binding (Holmes and Lehman, 2008; Lehman et al., 2019).

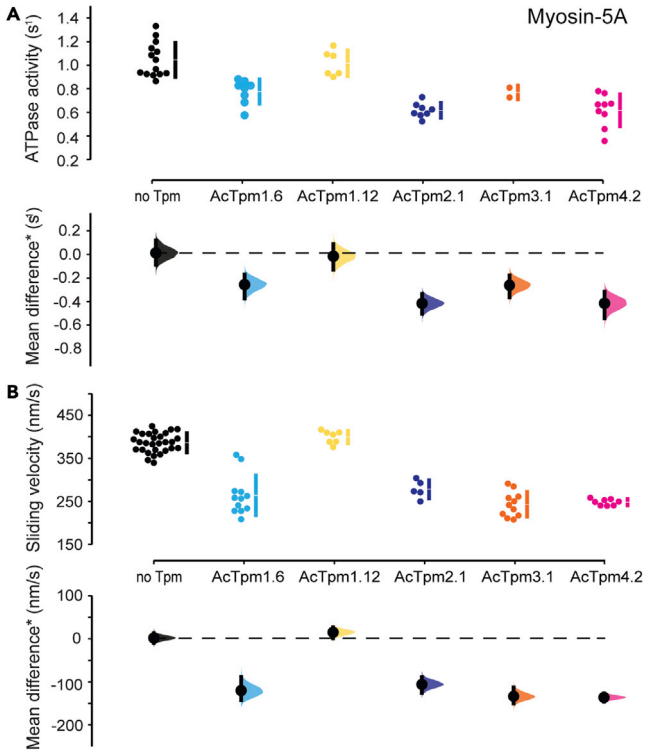

Figure 8. Changes in actin-activated ATP turnover and functional behavior of myosin-5A mediated by N-terminal acetylation of Tpm

(A) Cumming estimation plot showing the results of ATPase assays performed with 0.1-μM myosin-5A-HMM in the presence of filamentous β-actin ((20 μM) or A–Tpm cofilaments (20 μM). Two or more independent experiments, each involving at least four technical repeats, were performed for each experimental condition.

(B) Cumming estimation plot showing the results of *in vitro* motility assays performed with F-actin or A–Tpm cofilaments on surfaced decorated with myosin-5A-HMM. Five or more independent experiments, each involving at least five technical replicates with >100 trajectories, were performed for each experimental condition. All assays were performed at 30°C. The results of the individual measurements are shown as a swarmplot with mean ± standard deviation (SD) represented by a broken line. Effect sizes are shown as bootstrapped 95% confidence intervals (CI) on a separate, aligned axis. If the 95% CI contains the null value and the vertical bar is crossing the horizontal line of null effect, the combined results are considered not statistically different.

Gestalt-binding allows global changes in the position of Tpm cables as well as local positional perturbations caused by troponin, myosin or other actin-binding proteins and gives the A–Tpm cofilaments sufficient flexibility to allow alternative binding modes at a low-energy cost, while promoting tight cooperative coupling that is highly sensitive to allosteric trigger events such as post-translational modifications, protein–protein interactions, ligand binding, or isoform-specific amino acid substitutions (Fischer et al., 2016; Holmes and Lehman, 2008; Li et al., 2010). This provides the cell with a toolbox of modular components consisting of cofilaments containing different Tpm isoforms with and without post-translational modifications, capable of acting as mechanical sensors, selective tracks, for myosin motors and ultrasensitive switches. As mediators between chemical and mechanical signal transduction pathways, they enable cells to carry out precisely tuned reactions. The characterization of such systems requires an approach that incorporates accurate allosteric awareness overcoming difficulties in producing the correct combinations of protein isoforms with relevant post-translational modifications for the accurate determination of rate and equilibrium constants, structural features, forces, and velocities (Preller and Manstein, 2013). Therefore, we used contractile filaments composed of human cytoskeletal actin, myosin, and Tpm isoforms and produced the recombinant proteins without introducing any changes to their native sequence. Amino-terminally acetylated Tpm isoforms were produced in bacteria rather than the commonly used isoforms carrying a short N-terminal extension, such as Ala-Ser, to mimic acetylation. Phalloidin labeled with tetramethylrhodamine B isothiocyanate was used exclusively to stabilize and stain F-actin for *in vitro* motility assays, but omitted from all other assays.

Apart from the influence of post-translational modifications, Tpm binding to actin has been reported to be primarily dependent on exon usage (Cho and Hitchcock-DeGregori, 1991; Moraczewska et al., 1999; Pathan-Chhatbar et al., 2018; Schmidt et al., 2015). Variable exons 1 and 9, which specify residues contributing to the Tpm overlap complex, have been shown to affect actin affinity in the order 1b9d > 1b9a > Ac1a9a>1a9d≫1a9a≧1a9c≅1b9c in the context of recombinant Tpm1.3 smooth muscle variants that are identical except for the terminal regions encoded by exons 1a or 1b and exons 9a, 9c, or 9d (Pathan-Chhatbar et al., 2018). Exon 1a is expressed in muscle and non-muscle cells, whereas exon 1b replaces exons 1a and 2 in non-muscle cells, resulting in the production of LMW Tpm isoforms. The C-terminal exon 9a is expressed in striated muscles, endothelial cells, and in the brain, exon 9c exclusively in the brain, and exon 9d in non-muscle as well as in smooth muscle cells (Dufour et al., 1998; Schevzov et al., 2011; Vrhovski et al., 2003). Our results show for cytoskeletal Tpm isoforms that sequences contributing to the overlap region are not the sole determinant of differences in actin affinity. Changes for the non-acetylated LMW isoforms range from Tpm1.8(b.–.b.d; $K_{50\%}$: 0.10 μM), Tpm3.1(b.–.a.d; $K_{50\%}$: 1.50 μM), Tpm4.2(b.–.b.d; $K_{50\%}$: 1.99 μM), to Tpm1.12(b.–.b.c; $K_{50\%}$: ≥40 μM). The HMW isoforms Tpm1.6(a.b.b.d; $K_{50\%}$: 1.32 μM) and Tpm2.1(a.b.a.d; $K_{50\%}$: 1.73 μM) display actin affinities similar to the LMW isoforms Tpm3.1 and Tpm4.2. Regarding the role of variable exon six in shaping Tpm diversity in terms of A–Tpm interactions and cofilament mechanical properties, a comparison of LMW isoforms Tpm3.1(b.–.a.d) and Tpm4.2(b.–.b.d) and the HMW isoforms Tpm1.6(a.b.b.d) and Tpm2.1(a.b.a.d) shows that global sequence differences between the four *TPM* genes are of greater importance than variable exon 6 usage. Moreover, the differences that can be attributed to exon six usage are comparable in extent with those mediated by the presence or absence of N-terminal acetylation. The weakest binding to F-actin was observed with the use of exon 9c by Tpm1.12(b.–.b.c).

Our investigations of the temperature-dependent dissociation and reassociation of human cytoskeletal A–Tpm cofilaments revealed Tpm isoform-specific differences in T_{diss}, as well as differences in the extent of hysteresis exhibited by the dissociation and reassociation reactions, and the effects of N-terminal acetylation. Whereas, in the absence of N-terminal acetylation, the T_{diss} values of the HMW isoforms Tpm1.6 and Tpm2.1 exceeded those measured for the LMW isoforms Tpm3.1 and Tpm4.2 by 1°–6 °C, the opposite was true for the isoforms with N-terminal acetylation. Compared with an increase of T_{diss} by 10°–13 °C upon acetylation of Tpm3.1 and Tpm4.2, acetylation of Tpm1.6 and Tpm2.1 leads to a reduction of T_{diss} by 1°–2 °C. In line with the kinetic binding model of Tpm molecules to actin (Bareja et al., 2020), the greater thermal stability of A–Tpm can be explained by stronger end-to-end contacts of Tpm molecules. Alternative explanations include stronger coordination of Tpm assembly on actin filaments or greater flexibility of Tpm cables. Both lead to changes in gap formation, which have been described as sites of dissociation (Orzechowski et al., 2014; Schmidt et al., 2015). The number of gaps is thought to be controlled by Tpm concentration (Schmidt et al., 2015), which is consistent with our observation that changes in Tpm concentration affect the size of cooperative units. Gap formation potentially provides an additional selectivity filter for Tpm-gated access of actin-binding proteins to cytoskeletal F-actin. This is evident from differences in the exchange of free Tpm3.1 and Tpm4.2 with Tpm isoforms bound to F-actin. The much stronger effect of N-terminal acetylation on the temperature stability of A–Tpm containing LMW–Tpm isoforms compared with HMW–Tpm isoforms suggests that changes within the overlap region of Tpm cables lead to analogous differences in allosteric communication.

A comparison of our results obtained with the acetylated and non-acetylated isoforms of Tpm1.6, Tpm1.12, and Tpm4.2 (Table 1) and the reported T_{diss} and $K_{50\%}$ values for the corresponding Ala–Ser–tagged isoforms reveals minor changes (Marchenko et al., 2021). Thus, Ala–Ser labeling may have an influence on allosteric communication and cooperative coupling in A–Tpm cofilaments that remains to be confirmed, but is not required for efficient binding of these cytoskeletal Tpm isoforms to F-actin.

Functional diversification of cytoskeletal A–Tpm cofilaments and A–Tpm–M complexes

Tpm-specific regulation of cytoskeletal myosin isoforms has been described as being dependent on the myosin isoform or myosin class involved (Barua et al., 2014; Clayton et al., 2014, 2015; Kee et al., 2015; Pathan-Chhatbar et al., 2018). It has been proposed that A–Tpm3.1 cofilaments limit or block motor function, allowing Myo1C to perform its cellular functions only in areas containing bare actin filaments (Kee et al., 2015). In the presence of cytoskeletal A–Tpm cofilaments including A–Tpm3.1, our results show up to 80% slower sliding velocities, a 27–38% decrease in k_{cat} and marked reductions in force generation. However, as the apparent affinity of Myo1C for F-actin in the presence of ATP (K_{app}) remains unchanged in the presence of saturating concentration of cytoskeletal Tpm isoforms, we favor a role for the cytoskeletal

A–Tpm cofilaments where they interact productively with human Myo1C by shifting motor activity from faster movement on bare F-actin to more efficient tension sensing on A-Tpm cofilaments. Such a shift is consistent with the distinct roles of Myo1C in transport, storage, and insertion of GLUT4 vesicles into the plasma membrane (Boguslavsky et al., 2012).

Based on the event frequency, run length, and unloaded velocity, actin–Tpm3.1 and actin–Tpm1.8 cofilaments were described as equal or better tracks compared with bare actin for murine myosin 5A-HMM. In contrast, actin–Tpm4.2 was described to exclude myosin-5A-HMM from productive interactions (Sckolnick et al., 2016). Our results show more subtle changes supporting graded functional adjustments as a consequence of an exchange of Tpm isoform. Under the experimental conditions used, both the rate of ATP turnover and the sliding velocity supported by human myosin-5A show significant reductions for most tested cytoskeletal Tpm isoforms with and without N-terminal acetylation. The exception is Tpm1.12 showing a significant increase in sliding velocity. Taking also into account the observed changes in run lengths, a uniformly high event frequency for all cofilament combinations examined, and the limitations of the assays used, we conclude that our results are dominated by a cofilament-specific modulation of the myosin-5A duty ratio. Therefore, exactly how motile and contractile activities play out in a cellular environment will depend on several other parameters, including local variations in motor density, external load, spatial constraints, and the presence of actin-binding auxiliary proteins.

Unlike the two other myosin isoforms tested, NM-2A shows increased enzymatic activity in the presence of most of the A–Tpm cofilaments tested. The extent of the enhancement of ATPase activity and sliding velocity varied for the different Tpm isoforms as well as with their N-terminal acetylation status. The largest changes in ATP turnover kinetics and the fastest sliding velocities were observed for A–Tpm cofilaments containing either Tpm3.1 or AcTpm3.1. Cofilaments containing AcTpm1.6 and AcTpm4.2 moved significantly faster compared to the non-acetylated isoforms and bare F-actin. Cofilaments containing AcTpm2.1 displayed a small but significant increase in velocity only over bare F-actin. These findings provide a more nuanced picture compared with the previously reported enhanced NM-2A-dependent motor activity of A–Tpm cofilaments containing LMW Tpm3.1 and Tpm4.2 and a reduced productive interaction of cofilaments containing HMW Tpm1.6 and Tpm2.1 with NM-2A (Gateva et al., 2017). Inclusion of the N-terminally acetylated isoforms increases the physiologically relevance of our results.

Collectively, our ensemble kinetics values provide accurate descriptions of the effects of Tpm isoform exchange or changes in Tpm-acetylation status on the maximum rate of ATP turnover, the apparent affinity for the filament track in the presence of ATP, and the strength of the coupling between binding to filament tracks and the acceleration of rate-limiting steps in the actomyosin ATPase cycle. Opposing changes in the catalysis of ATP turnover and motor activity can be attributed to isoform-specific allosteric coupling between the different components of A–Tpm–M complexes that is responsive to the extent of saturation at which the solution kinetics and *in vitro* motility experiments are performed and to the surface density and arrangement of myosin motors in the *in vitro* motility assays (Hundt et al., 2016; Pertici et al., 2018; Toyoshima et al., 1989; Uyeda et al., 1990). Our results show how motor properties such as maximum velocity in the absence and presence of external loads and optimal motor density for continuous unidirectional motion, previously considered specific and invariant properties of each myosin isoform, are modulated by the presence of different Tpm isoforms as well as their post-translational modification. This provides a solid and indispensable foundation for future studies aimed at discovering small molecule therapeutics for the treatment of non-muscular myosinopathies and actinopathies.

Limitations of the study

The scope of our study is limited by the allosteric nature of the system under investigation, with the existence of a large number of possible combinations of cytoskeletal actin, myosin, and Tpm isoforms. Our study is focused on the *in vitro* characterization of selected A–Tpm–M combinations. The examples presented in our work reveal important key aspects for the major isoforms. In addition, they define the range over which the functional properties of A–Tpm–M complexes typically vary, and they allow certain combinations of isoforms to be clustered into groups with similar properties. Overall, our work provides a starting point and framework for quantitative modeling of motor processes at the cellular level. To realize its full potential, further studies are needed that provide insights into the subcellular localization of related motor processes, the spatial distribution, density, and concentration of the individual components, and the impact of posttranslational modifications on their functional properties.

STAR★METHODS

Detailed methods are provided in the online version of this paper and include the following:

- KEY RESOURCES TABLE
- RESOURCE AVAILABILITY
  - Lead contact
  - Materials availability
  - Data and code availability
- EXPERIMENTAL MODEL AND SUBJECT DETAILS
- METHOD DETAILS
  - Reagents
  - Constructs and proteins
  - Antibodies
  - Cosedimentation assays
  - Light scattering assays
  - Kinetic measurements
  - Myosin motor activity assays
- QUANTIFICATION AND STATISTICAL ANALYSIS

SUPPLEMENTAL INFORMATION

Supplemental information can be found online at https://doi.org/10.1016/j.isci.2022.104484.

ACKNOWLEDGMENTS

Dedicated to the memory of Kenneth C. Holmes. The authors thank Peter W. Gunning for the cDNA of human Tpm1.6 and Tpm2.1 and for helpful discussions, Claudia Thiel and Hella Scharnhorst for excellent technical assistance. This work was supported by Deutsche Forschungsgemeinschaft grant MA1081/23–1(to D.J.M). D.J.M. is a member of the Cluster of Excellence RESIST (EXC 2155) with support from the DFG [Project ID: 39087428–B11] and the European Joint Project on Rare Diseases Consortium "PredACTINg" with support from the German Federal Ministry of Education and Research [Grant Agreement ID: 01GM1922B]. D.P.M. was supported by the University of Kent and funding from the Biotechnology and Biological Sciences Research Council (BB/S005544/1). Part of the work was carried out at the MHH Research Core Facilities for Laser Microscopy and Structural Biochemistry. T.R. and S.G were enrolled in the PhD program *Molecular Medicine* of Hannover Biomedical Research School (HBRS).

AUTHOR CONTRIBUTIONS

All authors discussed the results and contributed to the final manuscript; T.R. and S.G. purified proteins and performed experiments; T.R., S.G., J.N.G., and D.J.M. analyzed the data; T.R., S.G., and D.J.M. designed the figures; T.R., S.G., J.N.G., D.P.M., I.C., M.H.T. P.Y.R., and S.L.L. contributed to the experimental design, data interpretation, and manuscript preparation; T.R. and D.J.M. wrote the manuscript; D.J.M. conceived and coordinated the study, and was responsible for funding acquisition and project administration.

DECLARATION OF INTERESTS

The authors declare no competing interests.

INCLUSION AND DIVERSITY

While citing references scientifically relevant for this work, we also actively worked to promote gender balance in our reference list.

Received: January 18, 2022
Revised: May 2, 2022
Accepted: May 24, 2022
Published: July 15, 2022

REFERENCES

Adamek, N., Coluccio, L.M., and Geeves, M.A. (2008). Calcium sensitivity of the cross-bridge cycle of Myo1c, the adaptation motor in the inner ear. Proc. Natl. Acad. Sci. U S A *105*, 5710–5715. https://doi.org/10.1073/pnas.0710520105.

Arnesen, T., Van Damme, P., Polevoda, B., Helsens, K., Evjenth, R., Colaert, N., Varhaug, J.E., Vandekerckhove, J., Lillehaug, J.R., Sherman, F., and Gevaert, K. (2009). Proteomics analyses reveal the evolutionary conservation and divergence of N-terminal acetyltransferases from yeast and humans. Proc. Natl. Acad. Sci. U S A *106*, 8157–8162. https://doi.org/10.1073/pnas.0901931106.

Bareja, I., Wioland, H., Janco, M., Nicovich, P.R., Jégou, A., Romet-Lemonne, G., Walsh, J., and Böcking, T. (2020). Dynamics of Tpm1.8 domains on actin filaments with single-molecule resolution. Mol. Biol. Cell *31*, 2452–2462. https://doi.org/10.1091/mbc.E19-10-0586.

Barua, B., Nagy, A., Sellers, J.R., and Hitchcock-DeGregori, S.E. (2014). Regulation of nonmuscle myosin II by tropomyosin. Biochemistry *53*, 4015–4024. https://doi.org/10.1021/bi500162z.

Barua, B., Sckolnick, M., White, H.D., Trybus, K.M., and Hitchcock-DeGregori, S.E. (2018). Distinct sites in tropomyosin specify shared and isoform-specific regulation of myosins II and V. Cytoskeleton *75*, 150–163. https://doi.org/10.1002/cm.21440.

Boguslavsky, S., Chiu, T., Foley, K.P., Osorio-Fuentealba, C., Antonescu, C.N., Bayer, K.U., Bilan, P.J., and Klip, A. (2012). Myo1c binding to submembrane actin mediates insulin-induced tethering of GLUT4 vesicles. Mol. Biol. Cell *23*, 4065–4078. https://doi.org/10.1091/mbc.E12-04-0263.

Bonello, T.T., Janco, M., Hook, J., Byun, A., Appaduray, M., Dedova, I., Hitchcock-DeGregori, S., Hardeman, E.C., Stehn, J.R., Böcking, T., and Gunning, P.W. (2016). A small molecule inhibitor of tropomyosin dissociates actin binding from tropomyosin-directed regulation of actin dynamics. Sci. Rep. *6*, 19816. https://doi.org/10.1038/srep19816.

Brettle, M., Patel, S., and Fath, T. (2016). Tropomyosins in the healthy and diseased nervous system. Brain Res. Bull. *126*, 311–323. https://doi.org/10.1016/j.brainresbull.2016.06.004.

Bryce, N.S., Schevzov, G., Ferguson, V., Percival, J.M., Lin, J.J.-C., Matsumura, F., Bamburg, J.R., Jeffrey, P.L., Hardeman, E.C., Gunning, P., and Weinberger, R.P. (2003). Specification of actin filament function and molecular composition by tropomyosin isoforms. Mol. Biol. Cell *14*, 1002–1016. https://doi.org/10.1091/mbc.e02-04-0244.

Carman, P.J., Barrie, K.R., and Dominguez, R. (2021). Novel human cell expression method reveals the role and prevalence of posttranslational modification in nonmuscle tropomyosins. J. Biol. Chem. *297*, 101154. https://doi.org/10.1016/j.jbc.2021.101154.

Cho, Y.J., and Hitchcock-DeGregori, S.E. (1991). Relationship between alternatively spliced exons and functional domains in tropomyosin. Proc. Natl. Acad. Sci. U S A *88*, 10153–10157. https://doi.org/10.1073/pnas.88.22.10153.

Christensen, J.R., Hocky, G.M., Homa, K.E., Morganthaler, A.N., Hitchcock-DeGregori, S.E., Voth, G.A., and Kovar, D.R. (2017). Competition between Tropomyosin, Fimbrin, and ADF/Cofilin drives their sorting to distinct actin filament networks. Elife *6*. https://doi.org/10.7554/eLife.23152.

Clayton, J.E., Pollard, L.W., Murray, G.G., and Lord, M. (2015). Myosin motor isoforms direct specification of actomyosin function by tropomyosins. Cytoskeleton (Hoboken) *72*, 131–145. https://doi.org/10.1002/cm.21213.

Clayton, J.E., Pollard, L.W., Sckolnick, M., Bookwalter, C.S., Hodges, A.R., Trybus, K.M., and Lord, M. (2014). Fission yeast tropomyosin specifies directed transport of myosin-V along actin cables. Mol. Biol. Cell *25*, 66–75. https://doi.org/10.1091/mbc.E13-04-0200.

Coulton, A., Lehrer, S.S., and Geeves, M.A. (2006). Functional homodimers and heterodimers of recombinant smooth muscle tropomyosin. Biochemistry *45*, 12853–12858. https://doi.org/10.1021/bi0613224.

Cumming, G. (2011). Understanding the New Statistics : Effect Sizes, Confidence Intervals, and Meta-Analysis (Routledge).

De La Cruz, E.M., Wells, A.L., Rosenfeld, S.S., Ostap, E.M., and Sweeney, H.L. (1999). The kinetic mechanism of myosin V. Proc. Natl. Acad. Sci. U S A *96*, 13726–13731. https://doi.org/10.1073/pnas.96.24.13726.

Diensthuber, R.P., Müller, M., Heissler, S.M., Taft, M.H., Chizhov, I., and Manstein, D.J. (2011). Phalloidin perturbs the interaction of human non-muscle myosin isoforms 2A and 2C1 with F-actin. FEBS Lett. *585*, 767–771. https://doi.org/10.1016/j.febslet.2011.01.042.

Dufour, C., Weinberger, R.P., and Gunning, P. (1998). Tropomyosin isoform diversity and neuronal morphogenesis. Immunol. Cell Biol. *76*, 424–429. https://doi.org/10.1046/j.1440-1711.1998.00765.x.

East, D.A., Sousa, D., Martin, S.R., Edwards, T.A., Lehman, W., and Mulvihill, D.P. (2011). Altering the stability of the Cdc8 overlap region modulates the ability of this tropomyosin to bind co-operatively to actin and regulate myosin. Biochem. J. *438*, 265–273. https://doi.org/10.1042/BJ20101316.

Eastwood, T.A., Baker, K., Brooker, H.R., Frank, S., and Mulvihill, D.P. (2017). An enhanced recombinant amino-terminal acetylation system and novel in vivo high-throughput screen for molecules affecting α-synuclein oligomerisation. FEBS Lett. *591*, 833–841. https://doi.org/10.1002/1873-3468.12597.

Eaton, B.L. (1976). Tropomyosin binding to F-actin induced by myosin heads. Science *192*, 1337–1339. https://doi.org/10.1126/science.131972.

Fischer, S., Rynkiewicz, M.J., Moore, J.R., and Lehman, W. (2016). Tropomyosin diffusion over actin subunits facilitates thin filament assembly. Struct. Dyn. *3*, 012002. https://doi.org/10.1063/1.4940223.

Furch, M., Geeves, M.A., and Manstein, D.J. (1998). Modulation of actin affinity and actomyosin adenosine triphosphatase by charge changes in the myosin motor domain. Biochemistry *37*, 6317–6326. https://doi.org/10.1021/bi972851y.

Gateva, G., Kremneva, E., Reindl, T., Kotila, T., Kogan, K., Gressin, L., Gunning, P.W., Manstein, D.J., Michelot, A., and Lappalainen, P. (2017). Tropomyosin isoforms specify functionally distinct actin filament populations in vitro. Curr. Biol. *27*, 705–713. https://doi.org/10.1016/j.cub.2017.01.018.

Geeves, M.a., Hitchcock-DeGregori, S.E., and Gunning, P.W. (2015). A systematic nomenclature for mammalian tropomyosin isoforms. J. Muscle Res. Cell Motil. *36*, 147–153. https://doi.org/10.1007/s10974-014-9389-6.

Geeves, M.A. (1989). Dynamic interaction between actin and myosin subfragment 1 in the presence of ADP. Biochemistry *28*, 5864–5871. https://doi.org/10.1021/bi00440a024.

Giese, S., Reindl, T., Reinke, P.Y.A., Zattelman, L., Fedorov, R., Henn, A., Taft, M.H., and Manstein, D.J. (2020). Mechanochemical properties of human myosin 1C are modulated by isoform-specific differences in the N-terminal extension. J. Biol. Chem. *296*. https://doi.org/10.1074/jbc.RA120.015187.

Gill, S.C., and von Hippel, P.H. (1989). Calculation of protein extinction coefficients from amino acid sequence data. Anal. Biochem. *182*, 319–326. https://doi.org/10.1016/0003-2697(89)90602-7.

Greaseri, M.L., and Gergely, J. (1971). Reconstitution of troponin activity from three protein components. J. Biol. Chem. *246*, 4226–4233. https://doi.org/10.1016/S0021-9258(18)62075-7.

Greenberg, M.J., and Moore, J.R. (2010). The molecular basis of frictional loads in the in vitro motility assay with applications to the study of the loaded mechanochemistry of molecular motors. Cytoskeleton (Hoboken) *67*, 273–285. https://doi.org/10.1002/cm.20441.

Greene, L.E., and Eisenberg, E. (1980). Cooperative binding of myosin subfragment-1 to the actin-troponin-tropomyosin complex. Proc. Natl. Acad. Sci. U S A *77*, 2616–2620. https://doi.org/10.1073/pnas.77.5.2616.

Greenfield, N.J., Stafford, W.F., and Hitchcock-DeGregori, S.E. (1994). The effect of N-terminal acetylation on the structure of an N-terminal tropomyosin peptide and alpha alpha-tropomyosin. Protein Sci. *3*, 402–410. https://doi.org/10.1002/pro.5560030304.

Gunning, P., O'neill, G., and Hardeman, E. (2008). Tropomyosin-based regulation of the actin cytoskeleton in time and space. Physiol. Rev. *1–35*. https://doi.org/10.1152/physrev.00001.2007.

Gunning, P.W., Schevzov, G., Kee, A.J., and Hardeman, E.C. (2005). Tropomyosin isoforms: divining rods for actin cytoskeleton function.

Trends Cell Biol. *15*, 333–341. https://doi.org/10.1016/j.tcb.2005.04.007.

Heald, R.W., and Hitchcock-DeGregori, S.E. (1988). The structure of the amino terminus of tropomyosin is critical for binding to actin in the absence and presence of troponin. J. Biol. Chem. *263*, 5254–5259.

Heissler, S.M., and Manstein, D.J. (2012). Functional characterization of the human myosin-7a motor domain. Cell. Mol. Life Sci. *69*, 299–311. https://doi.org/10.1007/s00018-011-0749-8.

Hendricks, M., and Weintraub, H. (1981). Tropomyosin is decreased in transformed cells. Proc. Natl. Acad. Sci. U S A *78*, 5633–5637. https://doi.org/10.1073/pnas.78.9.5633.

Hitchcock-DeGregori, S.E., and Heald, R.W. (1987). Altered actin and troponin binding of amino-terminal variants of chicken striated muscle alpha-tropomyosin expressed in Escherichia coli. J. Biol. Chem. *262*, 9730–9735.

Ho, J., Tumkaya, T., Aryal, S., Choi, H., and Claridge-Chang, A. (2019). Moving beyond P values: data analysis with estimation graphics. Nat. Methods *16*, 565–566. https://doi.org/10.1038/s41592-019-0470-3.

Holmes, K.C., and Lehman, W. (2008). Gestalt-binding of tropomyosin to actin filaments. J. Muscle Res. Cell Motil. *29*, 213–219. https://doi.org/10.1007/s10974-008-9157-6.

Hundt, N., Steffen, W., Pathan-Chhatbar, S., Taft, M.H., and Manstein, D.J. (2016). Load-dependent modulation of non-muscle myosin-2A function by tropomyosin 4.2. Sci. Rep. *6*, 20554. https://doi.org/10.1038/srep20554.

Ihnatovych, I., Migocka-Patrzalek, M., Dukh, M., and Hofmann, W.A. (2012). Identification and characterization of a novel myosin Ic isoform that localizes to the nucleus. Cytoskeleton *69*, 555–565. https://doi.org/10.1002/cm.21040.

Janco, M., Bonello, T.T., Byun, A., Coster, A.C.F., Lebhar, H., Dedova, I., Gunning, P.W., and Böcking, T. (2016). The impact of tropomyosins on actin filament assembly is isoform specific. BioArchitecture *6*, 61–75. https://doi.org/10.1080/19490992.2016.1201619.

Johnson, C.A., Brooker, H.R., Gyamfi, I., O'Brien, J., Ashley, B., Brazier, J.E., Dean, A., Embling, J., Grimsey, E., Tomlinson, A.C., et al. (2018). Temperature sensitive point mutations in fission yeast tropomyosin have long range effects on the stability and function of the actin-tropomyosin copolymer. Biochem. Biophys. Res. Commun. *506*, 339–346. https://doi.org/10.1016/j.bbrc.2017.10.109.

Kabbage, M., Trimeche, M., ben Nasr, H., Hammann, P., Kuhn, L., Hamrita, B., and Chahed, K. (2013). Tropomyosin-4 correlates with higher SBR grades and tubular differentiation in infiltrating ductal breast carcinomas: an immunohistochemical and proteomics-based study. Tumor Biol. *34*, 3593–3602. https://doi.org/10.1007/s13277-013-0939-0.

Kee, A.J., Yang, L., Lucas, C.A., Greenberg, M.J., Martel, N., Leong, G.M., Hughes, W.E., Cooney, G.J., James, D.E., Ostap, E.M., et al. (2015). An actin filament population defined by the tropomyosin Tpm3.1 regulates glucose uptake. Traffic *16*, 691–711. https://doi.org/10.1111/tra.12282.

Kovács, M., Wang, F., Hu, A., Zhang, Y., and Sellers, J.R. (2003). Functional divergence of human cytoplasmic myosin II: kinetic characterization of the non-muscle IIA isoform. J. Biol. Chem. *278*, 38132–38140. https://doi.org/10.1074/jbc.M305453200.

Kron, S.J., and Spudich, J.A. (1986). Fluorescent actin filaments move on myosin fixed to a glass surface. Proc. Natl. Acad. Sci. U S A *83*, 6272–6276. https://doi.org/10.1073/pnas.83.17.6272.

Latham, S.L., Ehmke, N., Reinke, P.Y.A., Taft, M.H., Eicke, D., Reindl, T., Stenzel, W., Lyons, M.J., Friez, M.J., Lee, J.A., et al. (2018). Variants in exons 5 and 6 of ACTB cause syndromic thrombocytopenia. Nat. Commun. *9*, 4250. https://doi.org/10.1038/s41467-018-06713-0.

Lehman, W., Moore, J.R., Campbell, S.G., and Rynkiewicz, M.J. (2019). The effect of tropomyosin mutations on actin-tropomyosin binding: in search of lost time. Biophys. J. *116*, 2275–2284. https://doi.org/10.1016/j.bpj.2019.05.009.

Lehrer, S.S., and Kerwar, G. (1972). Intrinsic fluorescence of actin. Biochemistry *11*, 1211–1217. https://doi.org/10.1021/bi00757a015.

Levitsky, D.I., Rostkova, E.V., Orlov, V.N., Nikolaeva, O.P., Moiseeva, L.N., Teplova, M.V., and Gusev, N.B. (2000). Complexes of smooth muscle tropomyosin with F-actin studied by differential scanning calorimetry. Eur. J. Biochem. *267*, 1869–1877. https://doi.org/10.1046/j.1432-1327.2000.01192.x.

Li, X.E., Holmes, K.C., Lehman, W., Jung, H., and Fischer, S. (2010). The shape and flexibility of tropomyosin coiled coils: implications for actin filament assembly and regulation. J. Mol. Biol. *395*, 327–339. https://doi.org/10.1016/j.jmb.2009.10.060.

Lin, J.J.C., Warren, K.S., Wamboldt, D.D., Wang, T., and Lin, J.L.C. (1997). Tropomyosin isoforms in nonmuscle cells. Int. Rev. Cytol. *170*, 1–39. https://doi.org/10.1016/s0074-7696(08)61619-8.

Manstein, D.J., and Mulvihill, D.P. (2016). Tropomyosin-mediated regulation of cytoplasmic myosins. Traffic *17*, 872–877. https://doi.org/10.1111/tra.12399.

Marchenko, M., Nefedova, V., Artemova, N., Kleymenov, S., Levitsky, D., and Matyushenko, A. (2021). Structural and functional peculiarities of cytoplasmic tropomyosin isoforms, the products of TPM1 and TPM4 genes. Int. J. Mol. Sci. *22*, 5141. https://doi.org/10.3390/ijms22105141.

Marston, S.B., Copeland, O., Messer, A.E., MacNamara, E., Nowak, K., Zampronio, C.G., and Ward, D.G. (2013). Tropomyosin isoform expression and phosphorylation in the human heart in health and disease. J. Muscle Res. Cell Motil. *34*, 189–197. https://doi.org/10.1007/s10974-013-9347-8.

Maytum, R., Geeves, M.A., and Konrad, M. (2000). Actomyosin regulatory properties of yeast tropomyosin are dependent upon N-terminal modification †. Biochemistry *39*, 11913–11920. https://doi.org/10.1021/bi000977g.

Maytum, R., Konrad, M., Lehrer, S.S., and Geeves, M.A. (2001). Regulatory properties of tropomyosin effects of length, isoform, and N-terminal sequence. Biochemistry *40*, 7334–7341. https://doi.org/10.1021/bi010072i.

McIntosh, B.B., Holzbaur, E.L.F., and Ostap, E.M. (2015). Control of the initiation and termination of kinesin-1-driven transport by myosin-Ic and nonmuscle tropomyosin. Curr. Biol. *25*, 523–529. https://doi.org/10.1016/j.cub.2014.12.008.

McLachlan, A.D., and Stewart, M. (1976). The 14-fold periodicity in alpha-tropomyosin and the interaction with actin. J. Mol. Biol. *103*, 271–298.

Mehta, A.D., Rock, R.S., Rief, M., Spudich, J.A., Mooseker, M.S., and Cheney, R.E. (1999). Myosin-V is a processive actin-based motor. Nature *400*, 590–593. https://doi.org/10.1038/23072.

Meiring, J.C.M., Bryce, N.S., Lastra Cagigas, M., Benda, A., Whan, R.M., Ariotti, N., Parton, R.G., Stear, J.H., Hardeman, E.C., and Gunning, P.W. (2019). Colocation of Tpm3.1 and myosin IIa heads defines a discrete subdomain in stress fibres. J. Cell Sci. *132*. https://doi.org/10.1242/jcs.228916.

Meiring, J.C.M., Bryce, N.S., Wang, Y., Taft, M.H., Manstein, D.J., Liu Lau, S., Stear, J., Hardeman, E.C., and Gunning, P.W. (2018). Co-polymers of actin and tropomyosin account for a major fraction of the human actin cytoskeleton. Curr. Biol. *28*, 2331–2337.e5. https://doi.org/10.1016/j.cub.2018.05.053.

Monteiro, P.B., Lataro, R.C., Ferro, J.A., and Reinach, F. de C. (1994). Functional alpha-tropomyosin produced in Escherichia coli. A dipeptide extension can substitute the amino-terminal acetyl group. J. Biol. Chem. *269*, 10461–10466.

Moraczewska, J., Nicholson-Flynn, K., and Hitchcock-Degregori, S.E. (1999). The ends of tropomyosin are major determinants of actin affinity and myosin subfragment 1-induced binding to F-actin in the open state. Biochemistry *38*, 15885–15892. https://doi.org/10.1021/bi991816j.

Müller, M., Diensthuber, R.P., Chizhov, I., Claus, P., Heissler, S.M., Preller, M., Taft, M.H., and Manstein, D.J. (2013). Distinct functional interactions between actin isoforms and nonsarcomeric myosins. PLoS One *8*, e70636. https://doi.org/10.1371/journal.pone.0070636.

Münnich, S., and Manstein, D.J. (2013). Expression, purification, crystallization and preliminary X-ray crystallographic analysis of human myosin 1c in complex with calmodulin. Acta Crystallogr. Sect. F. Struct. Biol. Cryst. Commun. *69*, 1020–1022. https://doi.org/10.1107/S1744309113020988.

Münnich, S., Taft, M.H., and Manstein, D.J. (2014). Crystal structure of human myosin 1c–the motor in GLUT4 exocytosis: implications for Ca2+ regulation and 14-3-3 binding. J. Mol. Biol. *426*, 2070–2081. https://doi.org/10.1016/j.jmb.2014.03.004.

Ngo, K.X., Umeki, N., Kijima, S.T., Kodera, N., Ueno, H., Furutani-Umezu, N., Nakajima, J., Noguchi, T.Q.P., Nagasaki, A., Tokuraku, K., and Uyeda, T.Q.P. (2016). Allosteric regulation by cooperative conformational changes of actin filaments drives mutually exclusive binding with

cofilin and myosin. Sci. Rep. *6*, 35449. https://doi.org/10.1038/srep35449.

Noguchi, T.Q.P., Kanzaki, N., Ueno, H., Hirose, K., and Uyeda, T.Q.P. (2007). A novel system for expressing toxic actin mutants in Dictyostelium and purification and characterization of a dominant lethal yeast actin mutant. J. Biol. Chem. *282*, 27721–27727. https://doi.org/10.1074/jbc.M703165200.

Nowak, G., Pestic-Dragovich, L., Hozák, P., Philimonenko, A., Simerly, C., Schatten, G., and de Lanerolle, P. (1997). Evidence for the presence of myosin I in the nucleus. J. Biol. Chem. *272*, 17176–17181. https://doi.org/10.1074/jbc.272.27.17176.

Orzechowski, M., Li, X.E., Fischer, S., and Lehman, W. (2014). An atomic model of the tropomyosin cable on F-actin. Biophys. J. *107*, 694–699. https://doi.org/10.1016/j.bpj.2014.06.034.

Palm, T., Greenfield, N.J., and Hitchcock-DeGregori, S.E. (2003). Tropomyosin ends determine the stability and functionality of overlap and troponin T complexes. Biophys. J. *84*, 3181. https://doi.org/10.1016/S0006-3495(03)70042-3.

Parry, D.A.D., and Squire, J.M. (1973). Structural role of tropomyosin in muscle regulation: analysis of the X-ray diffraction patterns from relaxed and contracting muscles. J. Mol. Biol. *75*, 33–55. https://doi.org/10.1016/0022-2836(73)90527-5.

Pathan-Chhatbar, S., Taft, M.H., Reindl, T., Hundt, N., Latham, S.L., and Manstein, D.J. (2018). Three mammalian tropomyosin isoforms have different regulatory effects on nonmuscle myosin-2B and filamentous β-actin *in vitro*. J. Biol. Chem. *293*, 863–875. https://doi.org/10.1074/jbc.M117.806521.

Pelham, R.J., Lin, J.J., and Wang, Y.L. (1996). A high molecular mass non-muscle tropomyosin isoform stimulates retrograde organelle transport. J. Cell Sci. *109*, 981. LP – 989.

Pertici, I., Bongini, L., Melli, L., Bianchi, G., Salvi, L., Falorsi, G., Squarci, C., Bozó, T., Cojoc, D., Kellermayer, M.S.Z., et al. (2018). A myosin II nanomachine mimicking the striated muscle. Nat. Commun. *9*, 3532. https://doi.org/10.1038/s41467-018-06073-9.

Pittenger, M.F., Kazzaz, J.A., and Helfman, D.M. (1994). Functional properties of non-muscle tropomyosin isoforms. Curr. Opin. Cell Biol. *6*, 96–104. https://doi.org/10.1016/0955-0674(94)90122-8.

Pleines, I., Woods, J., Chappaz, S., Kew, V., Foad, N., Ballester-Beltrán, J., Aurbach, K., Lincetto, C., Lane, R.M., Schevzov, G., et al. (2017). Mutations in tropomyosin 4 underlie a rare form of human macrothrombocytopenia. J. Clin. Invest. *127*, 814–829. https://doi.org/10.1172/JCI86154.

Preller, M., and Manstein, D.J. (2013). Myosin structure, allostery, and mechano-chemistry. Structure *21*, 1911–1922. https://doi.org/10.1016/j.str.2013.09.015.

Redwood, C., and Robinson, P. (2013). Alpha-tropomyosin mutations in inherited cardiomyopathies. J. Muscle Res. Cell Motil. *34*, 285–294. https://doi.org/10.1007/s10974-013-9358-5.

Reumiller, C.M., Schmidt, G.J., Dhrami, I., Umlauf, E., Rappold, E., and Zellner, M. (2018). Gender-related increase of tropomyosin-1 abundance in platelets of Alzheimer's disease and mild cognitive impairment patients. J. Proteomics *178*, 73–81. https://doi.org/10.1016/j.jprot.2017.12.018.

Rock, R.S., Rief, M., Mehta, A.D., and Spudich, J.A. (2000). In vitro assays of processive myosin motors. Methods *22*, 373–381. https://doi.org/10.1006/METH.2000.1089.

Sao, K., Jones, T.M., Doyle, A.D., Maity, D., Schevzov, G., Chen, Y., Gunning, P.W., and Petrie, R.J. (2019). Myosin II governs intracellular pressure and traction by distinct tropomyosin-dependent mechanisms. Mol. Biol. Cell *30*, 1170–1181. https://doi.org/10.1091/mbc.E18-06-0355.

Schevzov, G., Whittaker, S.P., Fath, T., Lin, J.J., and Gunning, P.W. (2011). Tropomyosin isoforms and reagents. BioArchitecture *1*, 135–164. https://doi.org/10.4161/bioa.1.4.17897.

Schindelin, J., Arganda-Carreras, I., Frise, E., Kaynig, V., Longair, M., Pietzsch, T., Preibisch, S., Rueden, C., Saalfeld, S., Schmid, B., et al. (2012). Fiji: an open-source platform for biological-image analysis. Nat. Methods *9*, 676–682. https://doi.org/10.1038/nmeth.2019.

Schmidt, W.M., Lehman, W., and Moore, J.R. (2015). Direct observation of tropomyosin binding to actin filaments. Cytoskeleton (Hoboken) *72*, 292–303. https://doi.org/10.1002/cm.21225.

Sckolnick, M., Krementsova, E.B., Warshaw, D.M., and Trybus, K.M. (2016). Tropomyosin isoforms bias actin track selection by vertebrate myosin Va. Mol. Biol. Cell *27*, 2889. https://doi.org/10.1091/MBC.E15-09-0641.

Silva, R.D., and Martinho, R.G. (2015). Developmental roles of protein N-terminal acetylation. Proteomics *15*, 2402–2409. https://doi.org/10.1002/pmic.201400631.

Spudich, J.A., Huxley, H.E., and Finch, J.T. (1972). Regulation of skeletal muscle contraction. II. Structural studies of the interaction of the tropomyosin-troponin complex with actin. J. Mol. Biol. *72*, 619–632.

Spudich, J.A., and Watt, S. (1971). The regulation of rabbit skeletal muscle contraction. I. Biochemical studies of the interaction of the tropomyosin-troponin complex with actin and the proteolytic fragments of myosin. J. Biol. Chem. *246*, 4866–4871.

Stefen, H., Suchowerska, A.K., Chen, B.J., Brettle, M., Kuschelewski, J., Gunning, P.W., Janitz, M., and Fath, T. (2018). Tropomyosin isoforms have specific effects on the transcriptome of undifferentiated and differentiated B35 neuroblastoma cells. FEBS Open Biol. *8*, 570–583. https://doi.org/10.1002/2211-5463.12386.

Stehn, J.R., Haass, N.K., Bonello, T., Desouza, M., Kottyan, G., Treutlein, H., Zeng, J., Nascimento, P.R.B.B., Sequeira, V.B., Butler, T.L., et al. (2013). A novel class of anticancer compounds targets the actin cytoskeleton in tumor cells. Cancer Res. *73*, 5169–5182. https://doi.org/10.1158/0008-5472.CAN-12-4501.

Tobacman, L.S. (2008). Cooperative binding of tropomyosin to actin. Adv. Exp. Med. Biol. *644*, 85–94. https://doi.org/10.1007/978-0-387-85766-4_7.

Toyoshima, Y.Y., Toyoshima, C., and Spudich, J.A. (1989). Bidirectional movement of actin filaments along tracks of myosin heads. Nature *341*, 154–156. https://doi.org/10.1038/341154a0.

Urbancikova, M., and Hitchcock-DeGregori, S.E. (1994). Requirement of amino-terminal modification for striated muscle alpha-tropomyosin function. J. Biol. Chem. *269*, 24310–24315.

Uyeda, T.Q., Kron, S.J., and Spudich, J.A. (1990). Myosin step size. Estimation from slow sliding movement of actin over low densities of heavy meromyosin. J. Mol. Biol. *214*, 699–710. https://doi.org/10.1016/0022-2836(90)90287-V.

Vilfan, A. (2001). The binding dynamics of tropomyosin on actin. Biophys. J. *81*, 3146–3155. https://doi.org/10.1016/S0006-3495(01)75951-6.

von der Ecken, J., Müller, M., Lehman, W., Manstein, D.J., Penczek, P.A., and Raunser, S. (2015). Structure of the F-actin–tropomyosin complex. Nature *519*, 114–117. https://doi.org/10.1038/nature14033.

Vrhovski, B., Schevzov, G., Dingle, S., Lessard, J.L., Gunning, P., and Weinberger, R.P. (2003). Tropomyosin isoforms from the gamma gene differing at the C-terminus are spatially and developmentally regulated in the brain. J. Neurosci. Res. *72*, 373–383. https://doi.org/10.1002/jnr.10586.

Wegner, A. (1980). The interaction of α,α- and α,β-tropomyosin with actin filaments. FEBS Lett. *119*, 245–248. https://doi.org/10.1016/0014-5793(80)80263-8.

Wegner, A. (1979). Equilibrium of the actin-tropomyosin interaction. J. Mol. Biol. *131*, 839–853. https://doi.org/10.1016/0022-2836(79)90204-3.

Weigt, C., Wegner, A., and Koch, M.H. (1991). Rate and mechanism of the assembly of tropomyosin with actin filaments. Biochemistry *30*, 10700–10707.

Wolfenson, H., Meacci, G., Liu, S., Stachowiak, M.R., Iskratsch, T., Ghassemi, S., Roca-Cusachs, P., O'Shaughnessy, B., Hone, J., and Sheetz, M.P. (2016). Tropomyosin controls sarcomere-like contractions for rigidity sensing and suppressing growth on soft matrices. Nat. Cell Biol. *18*, 33–42. https://doi.org/10.1038/ncb3277.

Zattelman, L., Regev, R., Ušaj, M., Reinke, P.Y.A., Giese, S., Samson, A.O., Taft, M.H., Manstein, D.J., and Henn, A. (2017). N-terminal splicing extensions of the human MYO1C gene fine-tune the kinetics of the three full-length myosin IC isoforms. J. Biol. Chem. *292*, 17804–17818. https://doi.org/10.1074/jbc.M117.794008.

STAR★METHODS

KEY RESOURCES TABLE

REAGENT or RESOURCE	SOURCE	IDENTIFIER
Antibodies		
Mouse monoclonal antibody QIAexpress Penta•His	Qiagen	Cat#34650
Sheep polyclonal antibody TPM3/9d	Merck Millipore	Cat#AB5447
Sheep polyclonal antibody TPM1/1b	Merck Millipore	Cat#ABC499
Sheep polyclonal antibody TPM1/9d	Merck Millipore	Cat#AB5441
Donkey anti–sheep IgG–HRP secondary antibody	Santa Cruz Biotechnology	Cat#sc–2473
Rabbit polyclonal antibody D55Ac	Eurogentec	N/A
Bacterial and virus strains		
E. coli Rosetta pLys-S	Merck Millipore	Cat#70956
E. coli BL21(DE3)	Thermo Fisher Scientific	Cat#EC0114
E. coli DH10Bac	Thermo Fisher Scientific	Cat#10361012
Chemicals, peptides, and recombinant proteins		
Phalloidin–tetramethyl rhodamine B isothiocyanate	Merck Millipore	Cat#P1951
Myosin light chain kinase	Abcam	Cat#ab55674
Lactate dehydrogenase from rabbit muscle	Roche Diagnostics	Cat#10127876001
Pyruvate kinase from rabbit muscle	Roche Diagnostics	Cat#10128155001
Catalase from bovine liver	Merck Millipore	Cat#C9322
Glucose oxidase from *aspergillus niger*	Merck Millipore	Cat#G7141
Experimental models: Cell lines		
*Sf*9 cells adapted to Sf-900™ II SFM	Thermo Fisher Scientific	Cat#11496015
Oligonucleotides		
See Table S1 for oligonucleotide sequences		
Recombinant DNA		
Plasmid: pET–3a	Merck Millipore	Cat#69418
Plasmid: pET–3d	Merck Millipore	Cat#69421
Plasmid: pET–23a(+)	Merck Millipore	Cat#69771
Plasmid: pRHA-67	Daniel P. Mulvihill, University of Kent, Canterbury, UK	N/A
Plasmid: pFastBac 1	Thermo Fisher Scientific	Cat#10360014
Plasmid: pFastBac Dual	Thermo Fisher Scientific	Cat#10712024
Human Myo1C^{0}–ΔTH1 cDNA	Giese et al., 2020	NM_001080779.1; aa residues 1–856
Human NM–2A cDNA	Hundt et al., 2016	NM_002473.5 ; aa residues 1–1337
Human Myosin–5A cDNA	This paper	NM_000259.3; aa residues 1–1098
Human Calmodulin–1 cDNA	This paper	NM_001329922.1
Human non–muscle essential light chain (MYL6) cDNA	Hundt et al., 2016	NM_021019.4
Human non–muscle regulatory light chain (MYL12b) cDNA	Hundt et al., 2016	NM_001144944.1

(*Continued on next page*)

Continued

REAGENT or RESOURCE	SOURCE	IDENTIFIER
Human β–actin cDNA	Müller et al., 2013	NM_001101.3
Human γ–actin cDNA	Müller et al., 2013	NM_001199954.1
Human Tpm1.6 cDNA	This paper	NM_001018004.2
Human Tpm1.7 cDNA	This paper	NM_001018006.2
Human Tpm1.8 cDNA	Pathan-Chhatbar et al., 2018	NM_001301289.2
Human Tpm1.12 cDNA	Pathan-Chhatbar et al., 2018	NM_001018008.2
Human Tpm2.1 cDNA	This paper	NM_213674.1
Human Tpm3.1 cDNA	Pathan-Chhatbar et al., 2018	NM_153649.4
Human Tpm4.2 cDNA	Hundt et al., 2016	NM_003290.3
Fission yeast Naa10 cDNA	Eastwood et al., 2017	NM_001019732.2
Fission yeast Naa15 cDNA	Eastwood et al., 2017	NM_001023149.2
Fission yeast Naa20 cDNA	Eastwood et al., 2017	NM_001022913.2
Fission yeast Naa25 cDNA	Eastwood et al., 2017	NM_001021526.2
Software and algorithms		
ImageJ	Schindelin et al., 2012	https://imagej.nih.gov/ij/
ImageJ plugin *wrMTrck*	Jesper Søndergaard Pedersen (jsp@phage.dk)	https://www.phage.dk/plugins/wrmtrck.html
Python	Python Software Foundation	https://www.python.org/downloads/
DABEST plugin for Python	Ho et al., 2019	https://github.com/ACCLAB/DABEST-python
Kinetic Studio 4.07	TgK Scientific Limited, Bradford on Avon, UK	https://www.hi-techsci.com/instruments/kinetic-studio/
Origin Pro 9.55	Originlab, Massachusetts, USA	https://www.originlab.com/

RESOURCE AVAILABILITY

Lead contact

Further information and requests for resources and reagents should be directed to, and will be fulfilled by the corresponding author and Lead Contact, Dietmar J. Manstein (Manstein.Dietmar@MH-Hannover.de).

Materials availability

All unique/stable reagents generated in this study are available from the Lead Contact with a completed Materials Transfer Agreement.

Data and code availability

The published article includes all data generated or analyzed during this study. Any additional information required to reanalyze the data reported in this paper is available from the lead contact upon request. This paper does not report original code.

EXPERIMENTAL MODEL AND SUBJECT DETAILS

Sf9 *(Spodoptera frugiperda)* cells adapted to Sf-900™ II SFM were purchased from Thermo Fisher/Gibco (Cat#11496015) and used for the production of recombinant proteins according to the manufacturer's instructions and as described in the methods section.

METHOD DETAILS

Reagents

All chemicals and reagents were of the highest purity commercially available. ATP, *N*–(1–Pyrene)iodoacetamide), EGTA, HEPES, MOPS were purchased from (Merck KGaA, Darmstadt, Germany).

Constructs and proteins

Human Myo1C^{0}–ΔTH1 (UniProtKB - O00159–2; residues 1–856) was co–produced with CaM from pFastBac^{TM} dual vector and purified from *Sf9* cells using Immobilized Metal Affinity Chromatography (IMAC; Ni-NTA) and size exclusion chromatography (SEC; Superdex 200 10/300 column) as described earlier (Münnich et al., 2014). Additionally, human CaM was produced in *E. coli* Rosetta pLySs (DE3) using a pET–3a vector. The over–produced tag–free CaM was purified using an initial heat precipitation step. The cell lysate was incubated at 70°C in a water bath for 10 min to remove most contaminating proteins by denaturation and aggregation, while CaM remains stable and soluble. Following centrifugation for 30 min at 100,000 *g*, the supernatant was loaded onto a phenyl sepharose column, washed with 50 mM HEPES pH 7.5, 200 mM NaCl, 5 mM DTT, 4 mM $MgCl_2$, 1 mM EGTA and pure CaM was eluted with 50 mM HEPES pH7.5, 1 mM EGTA (Münnich and Manstein, 2013).

The HMM fragment of human NM–2A (UniProtKB - P35579) with C–terminal His8– and Avi–tags was over-produced in complex with non–muscle essential light chain (MYL6; UniProtKB - P60660) and regulatory light chain (MYL12b; UniProtKB - O14950) using the baculovirus/Sf9 system. Cells were harvested, lysed (50 mM HEPES pH 7.5, 200 mM NaCl, 15 mM MgCl2, 4 mM ATP, 0.3 mM EGTA, 0.3 mM EDTA, 5% Glycerol, 1mM DTT and protease inhibitor cocktail) by sonication and purified by IMAC and SEC (Superdex 200 10/300; 25mM Hepes pH 7.3, 200mM NaCl, 1mM EDTA, 1mM EGTA, 1mM DTT). NM–2A–HMM was phosphory-lated immediately prior to use at 30°C for 30 min. NM–2A–HMM was incubated with myosin light chain ki-nase at a stoichiometric ratio of 20:1 in a reaction mixture containing 20 mM MOPS pH 7.0, 50 mM KCl, 2 mM $MgCl_2$, 1 mM $CaCl_2$, 0.15 mM EGTA, 0.2 μM calmodulin, 2 mM DTT and 2 μM of each, ELC and RLC.

The HMM fragment (residues 1–1098, Cloning-Primer listed in Table S1) of human myosin–5A (UniProtKB - Q9Y4I1) with C–terminal His8– and Avi–tags was overproduced using the baculovirus/Sf9 system and purified in complex with calmodulin–1 (CaM) (UniProtKB - P0DP23) according to the protocol used for NM–2A HMM. The residues forming the HMM fragment of human myosin–5A are identical for the three isoforms produced by alternative splicing.

The human β–actin (UniProtKB P60709) and γ–actin (UniProtKB - P63261) isoforms were overproduced and purified using the baculovirus/Sf9 system as described for mouse β–actin (Noguchi et al., 2007). In brief, cells were lysed (20 mM Tris pH8, 50mM KCl, 5Mm $CaCl_2$, 4% Triton X-100, 1 mg/mL Tween 20, 1mM ATP, 10mM Imidazole, 1mM DTT) by sonication and incubated with His-tagged gelsolin (G4-6) overnight. The soluble fraction was incu-bated with Ni-NTA and actin was eluted via a chelator of Ca^{2+}, EGTA. Actin containing fractions were polymer-ized with 150 mM KCl and F-actin separated by centrifugation. F-actin resuspended and dialyzed (10-mM Tris pH8, 1mM $CaCl_2$, 50mM KCl, 1mM DTT) overnight. The polymerization-depolymerization procedure was repeated. Chicken skeletal muscle α-actin (UniProtKB - P68139) was purified according to the method of Lehrer and Kerwar with slight modifications (Diensthuber et al., 2011; Lehrer and Kerwar, 1972). Human Tpm1.6 (NCBI Reference Sequence NP_001018004.1), Tpm1.8 (NCBI Reference Sequence NP_001288218.1), Tpm1.12 (NCBI Reference Sequence NP_001018008.1), Tpm2.1 (NCBI Reference Sequence NP_998839.1), Tpm3.1 (NCBI Refer-ence Sequence NP_705935.1) and Tpm4.2 (NCBI Reference Sequence NP_003281.1) were produced tag–free in *E. coli*. The amino terminal–acetylated Tpm isoforms were produced using coexpression of Tpm1.12, Tpm3.1 or Tpm4.2 with the fission yeast NatA complex (Naa10, UniProtKB - Q9UTI3; Naa15, UniProtKB - O74985). Tpm1.6 and Tpm2.1 were coproduced in *E. coli* with the NatB complex (Naa20, UniProtKB - O74457; Naa25, UniProtKB - Q9Y809) (Eastwood et al., 2017). Oligonucleotide sequences used for cloning are listed in Table S1. *E. coli* lysates (50mM Hepes pH7.5, 200 mM NaCl, 5mM $MgCl_2$, 5mM DTT, 0.5 mg/mL lysozyme, protease inhibitor) after over-producing acetylated and non–acetylated Tpm1.6, Tpm2.1, Tpm3.1 and Tpm4.2 was heated up to 80°C for 10 min and cooled on ice. The soluble fraction was filtered and Tpm precipitated at the respective pI. The pre-cipitate was separated by centrifugation and resuspended in low salt buffer (20mM Tris pH7.2, 100mM NaCl, 5mM $MgCl_2$) for anion exchange chromatography. Tpm containing fractions were concentrated by precipitation. All vectors used for protein production were confirmed by sequencing. Protein concentration was determined using the Bradford assay and by recording protein absorbance spectra of the region from 240 to 400 nm with a UV–2600 spectrophotometer (Shimadzu Deutschland GmbH, Duisburg, Germany). Molar extinction coeffi-cients at 280 nm were calculated from the amino acid composition (Gill and von Hippel, 1989).

Antibodies

Antibodies used in this study include the mouse monoclonal antibody QIAexpress Penta•His, BSA–free (Qiagen, catalogue no. 34650); the Tpm-specific sheep polyclonal antibodies TPM3/9d (Merck Millipore, catalogue no. AB5447), TPM1/1b (Merck Millipore, catalogue no. ABC499), and TPM1/9d (Merck Millipore,

catalogue no. AB5441); donkey anti–sheep IgG–HRP secondary antibody (Santa Cruz Biotechnology, catalogue no. sc–2473). Rabbit polyclonal antibody D55Ac was raised against the peptide Ac–MDAIKKKMQMLKLD (Eurogentec, Seraing, Belgium). D55Ac specifically detects N–acetylated isoforms derived from *TPM1* and *TPM2* that share the use of exon 1a. The epitope is found in Tpm1.1, Tpm1.2, Tpm1.3, Tpm1.4, Tpm1.5, Tpm1.6, Tpm1.7, Tpm1.10, Tpm2.1, Tpm2.2, Tpm2.3, and Tpm2.4.

Cosedimentation assays

Affinities of the different Tpm isoforms for filamentous β–actin were analyzed by means of co–sedimentation assays. Varying Tpm concentrations (0 to 20 μM) were incubated with 5 μM filamentous β–actin for 30 min at 21°C in cosedimentation buffer (20 mM MOPS pH 7.0, 100 mM KCl and 5 mM $MgCl_2$). Ultracentrifugation was used to separate A–Tpm cofilaments from free Tpm (30 min, 100,000 *g* at 10°C). Supernatant and pellet fractions were subsequently resolved by sodium dodecyl sulphate–polyacrylamide gel electrophoresis. Protein bands were quantified by densitometry using a Bio–Rad ChemiDoc™ MP system (Bio–Rad Laboratories, Inc., Hercules, CA, USA) and the Fiji release of ImageJ software version 1.49s (Schindelin et al., 2012). Four independent experiments were carried out for each acetylated and non–acetylated Tpm isoform, each with four individual measurements. The binding coefficients ($K_{50\%}$) were determined by fitting the sigmoidal binding curves with the Hill equation.

Light scattering assays

It has been shown that the temperature–induced dissociation of A–Tpm cofilaments can be followed by changes in the intensity of the light scattering signal at 350 nm (Wegner, 1979). A Cary Eclipse fluorescence spectrophotometer and the Thermal Application Module (Agilent Technologies, Santa Clara, CA, U.S.A.) were used to record the change in the light scattering signal as a function of temperature. Heating and cooling rates were set to 0.5°C/min. The buffers used for light scattering assays contained 20 mM potassium phosphate pH 7.4 and 50 mM NaCl 5 μM actin and 10 μM Tpm. Control measurements performed at different Tpm concentrations in the absence of actin did not result in a change of the light scattering signal. After complete dissociation of Tpm from A–Tpm cofilaments, the light scattering signal equals the signal of bare F–actin. Assuming that A–Tpm cofilament dissociation and association correspond to a two-state process, the observed sigmoidal temperature dependences can be fitted with a Boltzmann function. The inflection points of the sigmoidal curves define the respective transition temperature T_{diss} and T_{ass} for the different Tpm isoforms.

Kinetic measurements

The regulatory light chain of NM–2A–HMM was phosphorylated for 30 min at 30 °C in kinase buffer (20-mM MOPS pH 7.0, 50-mM KCl, 2-mM $MgCl_2$, 0.15 -mM EGTA, 2-mM DTT) containing 1-mM $CaCl_2$, 0.2 μM CaM, 2 μM essential light chain (MYL6), 2-μM regulatory light chain (MYL12b), 1-mM ATP, and 50-nM myosin light chain kinase. The steady-state ATPase rates of NM–2A and myosin–5A were measured using an NADH-coupled assay (Furch et al., 1998) in ATPase buffer–I containing 0.5-μM NM–2A–HMM or 0.1 μM myosin–5A, 20 mM MOPS pH 7.3, 50 KCl, 5 mM $MgCl_2$, 1-mM ATP, 0.8-mM NADH, 0.5-mM phosphoenolpyruvate, 20 μg/mL lactate dehydrogenase, 50 μg/mL pyruvate kinase at 30°C. Steady-state ATP turnover by myosin–$1C^0$ was measured in ATPase buffer–II containing 0.1 μM Myo$1C^0$–ΔTH1, 25 mM HEPES pH 7.5, 50 mM KCl, 5 mM $MgCl_2$, 0.5 mM DTT, 1 mM ATP, 0.4 mM NADH, 0.5 mM phosphoenolpyruvate, 20 μg/mL lactate dehydrogenase and 50 μg/mL pyruvate kinase at 37°C. [A] or [A–Tpm] was varied over the range from 0 to 50 μM. The change in absorption at 340 nm was recorded in 96–well plates on a CLARIOstar Plus microplate reader (BMG Labtech, Ortenberg, Germany) (Giese et al., 2020). All combinations were tested with and without the addition of myosin, and the actin ATPase rate was then subtracted from the myosin ATPase rates. For titrations, increasing concentrations of filamentous actin were pre–incubated with the different Tpm isoforms for 30 min at room temperature, before addition to the assay mix. To ensure that Tpm is present in saturating concentration, 20 μM Tpm was added in all experiments. The parameters k_{cat}, $K_{app.actin}$, and $k_{cat}/K_{app\cdot actin}$ were obtained by fitting the data to the Michaelis–Menten equation. $K_{app.actin}$ is the apparent dissociation equilibrium constant for actin or actin–Tpm binding in the presence of ATP, k_{cat} gives the maximum value of the ATPase activity, and $k_{cat}/K_{app.actin}$ corresponds to the apparent second order rate constant for actin binding, which indicates the coupling efficiency between actin and nucleotide binding. At concentrations of actin much lower than $K_{app.actin}$, $k_{cat}/K_{app.actin}$ is well–defined by the slope of the initial linear part of the dependence. Estimation statistics are depicted as a Cumming estimation plot (Cumming, 2011; Ho et al., 2019). At least four independent ATPase assays

were performed with myosin–5A and at least six with NM–2A–HMM and Myo1C^0–ΔTH1. Three to five technical replicates were performed during each assay.

Transient kinetic experiments were performed at 20 °C in a buffer containing 25 mM HEPES, pH 7.5, 5 mM $MgCl_2$, 0.5 mM DTT, and 50 mM KCl using either a HiTech Scientific SF–61 DX or a HiTech SF–61 SX stopped–flow system (TgK Scientific Ltd, Bradford–on–Avon, U.K.) (Heissler and Manstein, 2012; Hundt et al., 2016; Pathan-Chhatbar et al., 2018). Kinetic parameters for the interaction of myosin motor domains with nucleotide and F–actin were analyzed in terms of the kinetic model shown for Myo1C^0–ΔTH1 in Figure 1C (Giese et al., 2020). Rate constants are referred to as k_{+n} and k_{-n}, respectively. Dissociation equilibrium constants are denoted as K_n. K_A represents the affinity of myosin for F–actin in the absence of nucleotide. The equilibrium constant K_α for the closed–to–open isomerization of the nucleotide binding pocket and the isomerization rate $k_{+\alpha}$ were determined by monitoring the fluorescence change during the ATP-induced dissociation of pyrene-labeled acto–Myo1C–ΔTH1 (130 nM) following mixing with 0.03 to 10 mM ATP. The observed fluorescence transients are best described by double exponentials. The data for the ratio of slow to fast phase amplitudes (A_{slow}/A_{fast}) plotted against the ATP concentration are best–fitted to a hyperbola, where the plateau value defines K_α. The dependence of $k_{obs,slow}$ on ATP concentration are best–fitted with a hyperbola, where the plateau values define $k_{+\alpha}$ (Giese et al., 2020). Kinetic Studio software (TgK Scientific Ltd., Bradford on Avon, UK) was used for initial data inspection and analysis of transient kinetic data. Detailed data analysis was performed with Origin Pro 9.55 (OriginLab Corporation, Northampton, MA, USA) graphing and data analysis software. Each data point corresponds to the average of 3 to 5 single measurements. Goodness–of–fit criteria were evaluated using the coefficient of determination R^2 and χ^2 tests as implemented in Origin Pro 9.55.

Myosin motor activity assays

Unloaded *in vitro* motility assays were performed as described (Kron and Spudich, 1986) with the following modifications. F–actin was labelled with phalloidin–tetramethyl rhodamine B isothiocyanate (Merck KGaA, Darmstadt, Germany) overnight at 4°C. To determine the appropriate conditions for fast and constant velocities, we performed initial titrations of motor activity with each myosin construct in the presence of labelled F–actin. We determined 0.2 mg/mL Myo1C^0–ΔTH1, 0.2 mg/mL NM–2A and 0.01 mg/mL myosin–5A as optimal concentrations. Where appropriate, actin was pre–incubated with 15 μM Tpm. In these cases, Tpm was added to all buffer solutions used. For His–tagged Myo1C^0–ΔTH1, one chamber volume (10 μL) of 0.05 mg/mL His antibody (QIAexpress® mouse monoclonal Penta·His^{TM}) was infused into the flow chamber and incubated for 5 min. Free positions on the surface were blocked with 0.5 mg/mL BSA in assay buffer (20 mM MOPS pH 7.3, 50 mM KCl, 5 mM $MgCl_2$). Actin sliding motility was measured at 30°C (NM–2A and myosin–5A) or 37°C (Myo1C^0–ΔTH1) using an Olympus IX70 or IX81 fluorescence microscope equipped with a 60×/1.49 NA PlanApo objective and an Orca Flash 4.0 CMOS camera (Hamamatsu Photonics, Herrsching, Germany). Independent *in vitro* motility assays were performed with two flow cells per isoform, where three or more video sequences of 180 s were recorded and at least 400 filaments were tracked per sequence. Sliding velocities were determined using the ImageJ plugin *wrMTrck* (Schindelin et al., 2012) and Origin V9.55 (OriginLab Corporation, Northampton, MA, USA). Estimation statistics are depicted as a Cumming estimation plot (Cumming, 2011; Ho et al., 2019). Frictional loading assays were performed in the presence of rising concentrations of α-actinin to generate increasing viscoelastic loads on the actin filaments and at a surface density of 3,600 Myo1C^0–ΔTH1 motors μm^{-2} (Greenberg and Moore, 2010). Results were analyzed according to (Ngo et al., 2016).

QUANTIFICATION AND STATISTICAL ANALYSIS

Estimation statistics for the results of kinetic and *in vitro* motility measurements were obtained using the DABEST plugin for Python (Ho et al., 2019) and depicted as a Cumming estimation plot, a variation of the Gardner– Altman Multi–group estimation plot (Cumming, 2011; Ho et al., 2019). Estimation statistics focuses on effect size measuring the strength of the relationship between two variables on a numeric scale. The results of the individual measurements are shown as a swarmplot with mean ± standard deviation (SD) represented by a broken line. Effect sizes are shown as bootstrapped 95% confidence intervals (CI) on a separate, aligned axis. If the 95% CI contains the null value and the vertical bar is crossing the horizontal line of null effect, the combined results are considered not statistically different.